Direct Modulation for Conventional Matrix Converters Using Analytical Signals and Barycentric Coordinates

PAWEL SZCZEPANKOWSKI[ID]**1, (Member, IEEE), TOMASZ BAJDECKI**[ID]**2,**
AND RYSZARD STRZELECKI[ID]**1, (Senior Member, IEEE)**
[1]Department of Power Electronics and Electrical Machines, Faculty of Electrical and Control Engineering, Gdansk University of Technology, 80-233 Gdańsk, Poland
[2]Institute of Power Engineering, 01-330 Warszawa, Poland

Corresponding author: Pawel Szczepankowski (pawel.szczepankowski@pg.edu.pl)

ABSTRACT This paper proposes the generalized direct modulation for Conventional Matrix Converters (CMC) using the concept of analytical signals and barycentric coordinates. The paper proposes a novel approach to the Pulse Width Modulation (PWM) duty cycle computing, which allows faster prototyping of direct control algorithms. The explanation of the new idea using analytical considerations demonstrating the principles of direct voltage synthesis has been presented in the article. The study concerns mainly the CMC3×3 but solutions for $3 \times n$, 5×5, and 5×3 topologies have also been discussed. The transformation of instantaneous input voltages to analytic signals great permits for simple presenting of real input voltage conditions such as waveform type, asymmetry or other deformation like higher–order harmonics. The proposed interpolation methods allow for determining the values of PWM duty cycles using simple formulas based on the determinants of the 2nd–degree matrices. Therefore, the proposed method, which based on the barycentric coordinates, frees an algorithm from trigonometry and angles.

INDEX TERMS Matrix converter, PWM computation, analytic signal, barycentric coordinates.

I. INTRODUCTION

To achieve a better understanding of the proposed concept of direct modulation, the introduction section was divided into two smaller subsections. The brief comparison between typical DC–AC inverters and the matrix converter topology has been presented first. That subsection contains some criticism stand of such concept and tries to explain why this kind of power converters are still interesting and perspective. The second subsection is devoted to the presentation of the issue of PWM duty cycle computation methods for multi–phase matrix converters controls by the direct method of modulation. In particular, this part of the Introduction indicates a problem with elaboration on the mathematical form of an equation for the PWM duty cycle when a number of CMC input is greater than 3 (e.g. 5, 12).

The associate editor coordinating the review of this manuscript and approving it for publication was Xavier Yang.
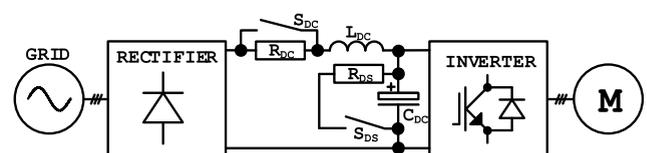

FIGURE 1. Typical VFD inverter.

A. A BRIEF LOOK AT THE MATRIX CONVERTER

Demands for energy savings have increased in recent years. This trend also means smaller size, high efficiency, the power density of the variable frequency drive (VFD) inverters.

Typical VFD, shown in Fig. 1, delivers power from the source – typically the constant frequency grid – to an electrical motor. This device converts an AC voltage into the DC voltage by the rectifier. A voltage smoothing bulk electrolytic capacitor in the DC-link circuit is required for this purpose. Capacitor bank stores the power, which is converted back into AC voltage with the desired frequency using the PWM inverter. As can be seen in Fig. 1, the DC–link requires
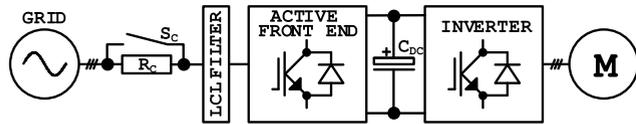
FIGURE 2. VFD with AFE inverter.

charge–up elements R_{DC} and S_{DC} to suppress the inrush high currents that flow to the uncharged electrolytic capacitor C_{DC}. The 6–pulse diodes bridge is cost–effective but produces grid current harmonics that are transferred back into the power system, resulting in additional heat and losses, and causing erratic behavior of connected equipment. Rectifiers (i.e. 12–pulse, 18–pulse, or 24–pulse) can reduce harmonics, but this solution is costly. Therefore the current smoothing L_{DC} reactor is installed to reduce the THD of the input currents. Moreover, the diode rectifier is a unidirectional device and a braking unit R_{DS}-S_{DS} should be used in order to dissipate the regenerated power from the electrical motor. This circuit also prevents dangerous increases in the over–voltage in the DC circuit. The described typical VFD inverter is economical but does not belong to the high–efficiency power devices. The generated input current harmonics are the main disadvantage of such a construction. Another solution to reduce harmonics is to add passive absorbing harmonic frequencies filters, which generally use more energy and for medium voltage applications are characterized by the large weight and volume. The VFD with an active front end (AFE) inverter, shown in Fig. 2, is a sensible and popular alternative recently. The AFE-VFD is a bidirectional power converter, which can generate the input current waveform and shapes it to be sinusoidal, reducing total harmonic distortion (THD) to 5 percent or less using the LCL filter. As for typical DC–AC inverters, the charge–up circuit R_C-S_C is still required.

The conventional matrix converter (CMC), illustrated in Fig. 3, arranges bidirectional switches into a matrix configuration (see Fig. 4), which permits for direct AC–AC voltage conversion, without DC–link [1]–[3]. Such topology, with a small input filter allows for realizing motor regeneration with negligible input current harmonic content. The practical realization of the single switch is of two IGBT's with two diodes or two RB–IGBT transistors [4]. There are other concepts of real bidirectional switch like the Full Bridge Sub–module used in M^3C converter, but such a proposition is a real cost challenge [5]. Note that, if the load current is interrupted, a large over–voltage upon the switch, can damage this semiconductor element. Thus, the dead time mechanism like in the conventional PWM inverter is applied and energy during this time interval is absorbed by the auxiliary protection circuit [6], [7]. From a pure industrial point of view – the real, not theoretical – a matrix topology, does not have a significant performance advantage over IGBT PWM inverters.

However, a four—quadrant model of CMC operation without the need for extra components, the near–sinusoidal input current, and no need for large reactive energy storage
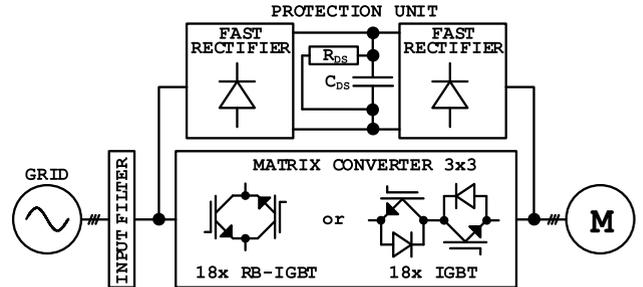

FIGURE 3. Conventional Matrix Converter circuit configuration.

parts, like electrolytic capacitors, makes matrix topology very perspective [8]. Note that the Gallium Nitride (GaN) and Silicon Carbide (SiC) semiconductors offer fundamental advantages over silicon solutions, in particular, the higher critical electrical field and smaller capacitances compared to silicon switches [9]–[12]. The switching frequency of these power semiconductors can be very high compared to the silicon counterparts, which makes these devices great for high–frequency application [13], [14]. The possibility of modulation with a very high PWM frequency can increase the efficiency of the matrix converter topology. In addition, required passive components will be smaller, thus a panel size of the CMC system can be significantly reduced. Attempts to integrate the CMC with the electric motor have already taken place [15]. It is another argument to further developed this topology. It can also be signaled that in addition to RB-IGBT technology, research is aimed at developing an equally good, as a not better, bidirectional switch. Ideal Power company (idealpower.com) is pioneering in bi-directional power switches Bi-polar Junction Transistor (B-TRAN) semiconductor technology. As we can read in the white paper, the B-TRAN is a unique double-sided bi-directional AC switch able to deliver substantial performance improvements over today's conventional power semiconductors. Ideal Power believes B-TRAN modules will reduce conduction and switching losses, complexity of thermal management and operating cost in medium voltage AC power switching and control circuitry.

Considering the advantages of matrix converters, such as the lack of a large DC capacitor, the bidirectional power flow, an input angle control, the undertaken research seems adequate [16].

B. DIRECT VOLTAGE SYNTHESIS IN MULTIPHASE SYSTEMS
The synthesis of the desired average k output voltage v_{ok}, in the CMC shown in Fig. 4, can be expressed by following a general formula

$$d_{1k} \cdot v_{i1} + d_{2k} \cdot v_{i2} + \cdots + d_{mk} \cdot v_{im} = v_{ok} \qquad (1)$$

where d_{1k}–d_{mk} are the non–negative PWM duty cycles, of which sum
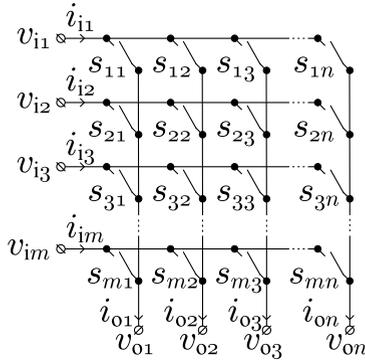
$$\sum_{j=1}^{m} d_{jk} = 1 \qquad (2)$$

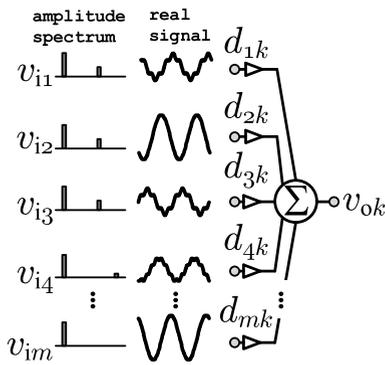**FIGURE 4.** The *m*–input and *n*–output Conventional Matrix Converter.

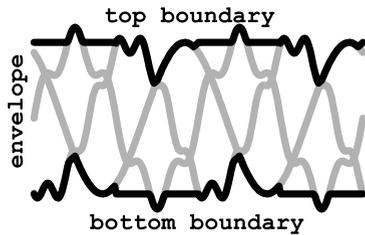**FIGURE 5.** An idea of *v*$_{ok}$ voltage synthesis.

FIGURE 6. Limitation of the output voltage synthesis.

is equal to unity by definition and in particular

$$d_{jk} = 1 \Leftrightarrow v_{ok} = v_{ij} \tag{3}$$

Summation scheme, which correspondes to the formula (1), is depicted in Fig. 5. The value of the reference output voltage v_{ok} must lie between the top boundary

$$v_{\max} = \max\{v_{i1}, \ldots, v_{im}\} \tag{4}$$

and the bottom boundary

$$v_{\min} = \min\{v_{i1}, \ldots, v_{im}\} \tag{5}$$

which shown in Fig. 6, where depicted envelope defines an available range of reference output value.

$$v_{\min} \leq v_{ok} \leq v_{\max} \tag{6}$$

No doubt, based on recent research progress, the v_{ok} can be generated using collections of PWM duty cycles calculated by various algorithms, which are widely reported in the

literature as a direct Venturini based methods, space vector approach [17], [18] or carrier–based modulation methods [1]–[3], [19]–[25]. A quite interesting approach to the AC-AC voltage synthesis represents the Model Predictive Control (MPC) with a finite control set and space vector modulation (SVM), which are the most common control methods for the CMC3 × 3 [23], [26], [27]. However, the possible range of PWM duty cycle values for *m* × *n* topology, is rarely discussed and analyzed in papers, moreover the general formula of direct AC–AC synthesis for any set of input voltages is not fully developed and demonstrated. Interest in multiphase electric machines and generators has rapidly increased in the last decade due to the desire to improve the reliability of the system, efficiency, and reduction of electromechanical moment ripple [28]–[30].

The final solutions formulated in the literature to date appear incomplete. The instantaneous reference output voltage changes have been presented as the trajectory in a two–dimensional coordinate system in [31]. While it has been concluded that the properties of the PWM modulation for CMC are closely related to the shape of that trajectory, the general formula of computing the PWM duty cycles has been not presented. In the next paper [32] the general approach of calculation of the PWM duty cycles has been demonstrated. The developed method used the intersection and projection techniques applied to the equilateral triangle, which modeled graphically the proposed solution of PWM duty cycles calculation. Despite the presented proposal, that has not been limited to the three output, a novel approach has focused finally on a balanced sinusoidal three–phase source case only, which has been expressed by an equilateral triangle, as noted above. Such a convex figure can not express more than three input phases or the abnormal input conditions including the non sinusoidal power supply. The generalized theory and analysis of scalar modulation techniques form CMC*m* × *n* has been presented in [33]. However, it has been found that the method was only extendable to 3 × *n* matrix converters.

The limitations of the above discussed approaches can be eliminated, to a great extend, by re–formulating the basis of AC–AC voltage synthesis. The paper at hand, presents a comprehensive study of generalized direct modulation using analytical signals and barycentric coordinates concepts.

The first section of the paper presents an analytical signal concept together with discussion of practical methods of analytic signal calculation. The PWM duty cycle computation using the barycentric coordinate concept is proposed in section II. Comprehensive theoretical analysis of the direct modulation for CMC3 × 3 and CMC3 × *n* is included and explained in section III. This section presents comparison between simulation and experimental results. Direct modulation schemes for multiphase conventional matrix converters with five inputs have been presented in section IV. Briefly summarizes and few conclusions have been included in the Conclusion section.

II. PRESENTATION OF AC VOLTAGES AS A COLLECTION OF ROTATING VECTORS USING THE ANALYTIC SIGNAL CONCEPT

Characterization and analysis of the AC voltage, in particular, the grid voltage, using an instantaneous amplitude, instantaneous phase, and instantaneous frequency are very important. This characterization fulfills important tasks in the integration of AC voltage source in the power grid such as synchronization, power flow control and power conversion quality. The presentation of AC voltages as a collection of rotating vectors using the analytic signal concept is proposed and described here.

The real measured and sampled voltage v_x can be transformed into analytic complex–valued signal written

$$\bar{v} = v_x + j \cdot v_y = v_x + j \cdot H(v_x) \tag{7}$$

where $j = \sqrt{-1}$ and letter H denotes the Hilbert transform defined as follows

$$H(v_x) = \frac{1}{\pi} \int_{-\pi}^{\pi} \frac{v_x(\tau)}{t - \tau} d\tau \tag{8}$$

This transform introduces a 90–degree phase shift to all sinusoidal components, which is illustrated in Fig. 7. Thus, in the discrete–time periodic–frequency domain, the transfer can be simply specified as

$$H(j\omega) = -H^{-1}(j\omega) = \begin{cases} -j & \omega > 0 \\ 0 & \omega = 0 \\ j & \omega < 0 \end{cases} \tag{9}$$

In relation to three–phase power supply, the sampled input voltages, which are usually the pure three sinusoids with pulsation ω_i,

$$
\begin{aligned}
v_{i1x} &= V \cos(\omega_i t) \\
v_{i2x} &= V \cos(\omega_i t - 2\pi/3) \\
v_{i3x} &= V \cos(\omega_i t + 2\pi/3)
\end{aligned} \tag{10}
$$

By generating a phase–quadrature components

$$
\begin{aligned}
v_{i1y} &= V \sin(\omega_i t) \\
v_{i2y} &= V \sin(\omega_i t - 2\pi/3) \\
v_{i3y} &= V \sin(\omega_i t + 2\pi/3)
\end{aligned} \tag{11}
$$

they can be converted to a collection of three rotating vectors

$$
\begin{aligned}
\bar{v}_{i1} &= V e^{j\omega_i t} \\
\bar{v}_{i2} &= V e^{j(\omega_i t - 2\pi/3)} \\
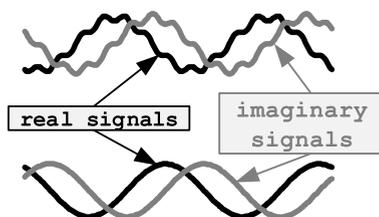\bar{v}_{i3} &= V e^{j(\omega_i t + 2\pi/3)}
\end{aligned} \tag{12}
$$

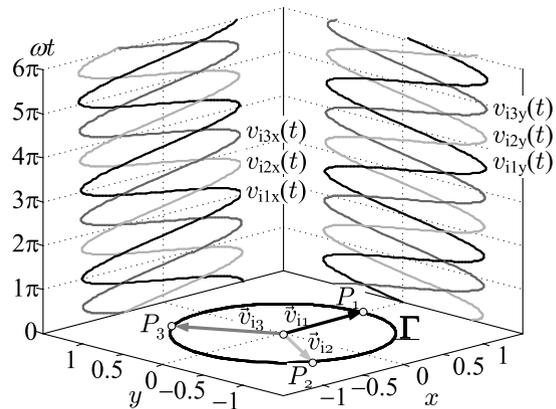**FIGURE 7.** An example waveforms of real and imaginary signals.

FIGURE 8. The three pure sinusoids representation by rotating vectors in *xy* reference frame.

shown in Fig. 8, by a well known quarter–cycle time shift method or using Clarke based triple transform as follows

$$
\begin{bmatrix} v_{i1x} & v_{i1y} \\ v_{i2x} & v_{i2y} \\ v_{i3x} & v_{i3y} \end{bmatrix} = \begin{bmatrix} v_{i1x} & v_{i2x} & v_{i3x} \\ v_{i2x} & v_{i3x} & v_{i1x} \\ v_{i3x} & v_{i1x} & v_{i2x} \end{bmatrix} \begin{bmatrix} 1 & 0 \\ 0 & 1/\sqrt{3} \\ 0 & -1/\sqrt{3} \end{bmatrix} \tag{13}
$$

In the text, the subscript 'i' denotes the input side of the converter while the subscript 'o' denotes the output side. Proposed expression (13) can be interpreted as quadrature components generator, which creates three virtual orthogonal reference frame. Note, that no trigonometry and angles based formulas have to be elaborated, thus the proposed algorithm takes a simple form and no Phase Lock Loop (PLL) is needed.

The calculation of analytical signals for AC unbalanced and distorted voltages requires the use of advanced operations. However, this should not be seen as disadvantage of the proposed approach, because the frequency analysis is widely implemented and supported in DSP processors and FPGA devices. When high precision of output voltage generation is needed, the accurate calculation of vectors coordinates requires the Hilbert Transform Filter [34] or operation based on Fast Fourier Transform (FFT) [35]. In many cases, the calculation can be limited to several dominant harmonics, thus the Discrete Fourier Transform (DFT) based approach, such as moving–window DFT, may be applied [36].

For further deliberation let's assume that all required analytical signals, which correspond to input voltages, have been calculated appropriately and any deterministic voltage deformations have been expressed by the Hilbert pairs represented by equation (7). Each sampled AC voltage is transformed into one point with coordinates *xy*. These points – either all or at least three selected – are vertices of the convex polygon, which is the voltage synthesis field. A similar proposal was introduced in [32] as the Duty Cycle Space Vectors concept, in which the synthesis field is presented only as of the stationary equilateral triangle, which does not rotate compared to the proposed method and can not express abnormal voltage conditions such as unbalance and higher–order harmonics.

For three–phase balanced sources the synthesis field can be easily constructed using (13). For symmetric and balanced multi–phase voltage sources the construction of the synthesis field is intuitive. If the input voltages are arbitrary and do not create symmetric voltage systems or contain higher harmonics, a precise AC–AC conversion requires special signal processing techniques, as reported earlier.
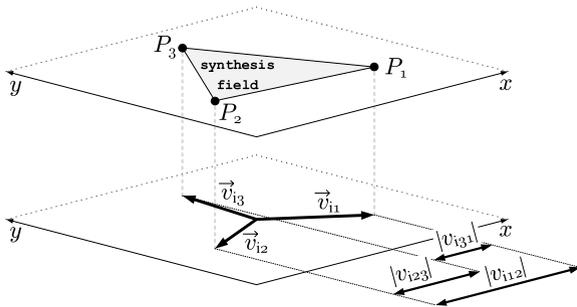

FIGURE 9. The synthesis field.

Note that the distances, shown in Fig. 9, between the x coordinates of the analytical voltage vectors are equal to the instantaneous line–to–line voltages. The differences between y coordinates define the boundaries of the combination of the input voltage share during the forming process the average output voltage. This situation is illustrated in Fig. 10, where considered boundaries are designated by triangle edges, while points P_4, P_5, and P_6 represented the three possible reference voltage location inside the synthesis field.

The *real* part of the reference analytical voltage (7) can be generated using the average value concept. This means, that in general, the average output voltage value is constructed based on the three fragments of supply voltages. These fragments differ from each other of the instantaneous voltage value. Two principle cases can be distinguished. The output voltage can be generated using only two input voltages. Point P_5 represents a voltage synthesis using the L1 and L3 input phase, while point P_4 indicates the solution based on the L1 and L2 input phase respectively. Point P_6 represents a general variant, which is the essence of the proposed approach. The output voltage is always generated using all three input voltages. The straight line between the point P_5 and P_4 constructs a geometrical change range for the y coordinate. By definition, this coordinate represents the imaginary part of the analytic signal and finally does not influence on the average fundamental output voltage [37].

However, to preserve the feature of matrix topology such as the sinusoidal current on both converter's sides, the value of the imaginary part of the reference output voltage has to be especially elaborated. Changes in the output voltage value represented by analytical form can be graphically demonstrated as the Γ trajectory, which is shown in Fig. 8 and corresponded to the input voltage collections. This issue will be discussed in a separate chapter. However, for a better understanding of the novel approach, the PWM duty cycle calculation method should be presented before.
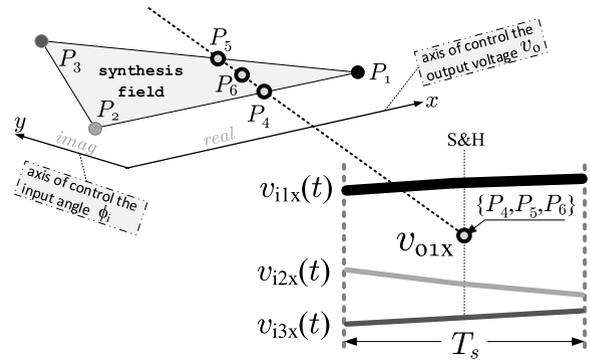

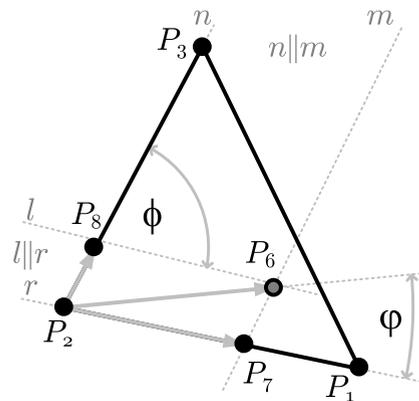**FIGURE 10.** The three possible reference location inside the synthesis field.

FIGURE 11. The general vectors arrangement for the geometrical solution using trigonometry and angles.

III. PWM DUTY CYCLE COMPUTATION USING BARYCENTRIC COORDINATES

This section has been divided into two parts. The first one has been addressed to the problem of PWM duty cycle computation for CMC3 × 3. An attempt to formulate a general computation scheme for the multiphase matrix converter has been proposed in the next subsection.

A. ELABORATION OF PWM DUTY CYCLES COMPUTING CONCEPT FOR CONVENTIONAL MATRIX CONVERTER

A mathematical expression for computing the PWM duty cycles can be constructed in an explicit algebraic form based on the triangle vertices coordinates in two–dimensional Cartesian reference frame [38]. Considering the vectors arrangement illustrated in Fig. 11, the points P_4 and P_5 represent two trivial cases, while the point P_6 – with the same x coordinate – designates the general output vector position $\vec{v}_{o1}$ in the synthesis field. The following proportions based on the sine rule applied to the shown geometry. They can be formulated as follows

$$\frac{|P_2 P_6|}{\sin (\pi - \phi)} = \frac{|P_2 P_8|}{\sin (\varphi)} = \frac{|P_2 P_7|}{\sin (\phi - \varphi)} \quad (14)$$

Duty cycles d_1 and d_3, which correspond to the points P_1 and P_3 respectively, can be calculated as a ratio of the absolute

value of the appropriate vector products as expressed below

$$d_1 = \frac{|P_2P_7|}{|P_2P_1|} = \frac{|P_2P_6|}{|P_2P_1|} \frac{\sin(\phi - \varphi)}{\sin(\phi)} \cdot \frac{|P_2P_3|}{|P_2P_3|} \quad (15)$$

$$d_3 = \frac{|P_2P_8|}{|P_2P_3|} = \frac{|P_2P_6|}{|P_2P_3|} \frac{\sin(\varphi)}{\sin(\phi)} \cdot \frac{|P_2P_1|}{|P_2P_1|} \quad (16)$$

which can be written as

$$d_1 = \frac{\left|\overrightarrow{P_2P_6} \times \overrightarrow{P_2P_3}\right|}{\left|\overrightarrow{P_2P_1} \times \overrightarrow{P_2P_3}\right|} \quad (17)$$

$$d_3 = \frac{\left|\overrightarrow{P_2P_6} \times \overrightarrow{P_2P_1}\right|}{\left|\overrightarrow{P_2P_3} \times \overrightarrow{P_2P_1}\right|} \quad (18)$$

Note, that the magnitude of the cross product of two vectors is the area of the parallelogram with the two vectors as adjacent sides. Thus equations (17) and (18) can be transformed finally to expression

$$d_1 = \xi \cdot \left| \det \begin{bmatrix} v_{i2x} - v_{o1x} & v_{i2y} - v_{o1y} \\ v_{i3x} - v_{o1x} & v_{i3y} - v_{o1y} \end{bmatrix} \right| = \frac{\Delta_{[2,6,3]}}{\Delta_{[1,2,3]}} \quad (19)$$

$$d_3 = \xi \cdot \left| \det \begin{bmatrix} v_{i1x} - v_{o1x} & v_{i1y} - v_{o1y} \\ v_{i2x} - v_{o1x} & v_{i2y} - v_{o1y} \end{bmatrix} \right| = \frac{\Delta_{[2,6,1]}}{\Delta_{[1,2,3]}} \quad (20)$$

where "det" means the determinant of the matrix 2×2, and

$$\xi = \left| \det \begin{bmatrix} v_{i2x} - v_{i1x} & v_{i2y} - v_{i1y} \\ v_{i3x} - v_{i1x} & v_{i3y} - v_{i1y} \end{bmatrix} \right|^{-1} \quad (21)$$

The value of d_2 can be computed in the same manner

$$d_2 = 1 - d_1 - d_3 = \frac{\Delta_{[3,6,1]}}{\Delta_{[1,2,3]}} \quad (22)$$

Thus angle and trigonometric functions have been eliminated from the algorithm. According to the obtained result, a novel approach for the PWM duty cycle computation may be performed using the arrangement of the triangles shown in Fig. 12, where equations (19) and (20) define barycentric coordinates. An analogous scheme of consideration can proceed to any convex polygon, in the meaning of the synthesis
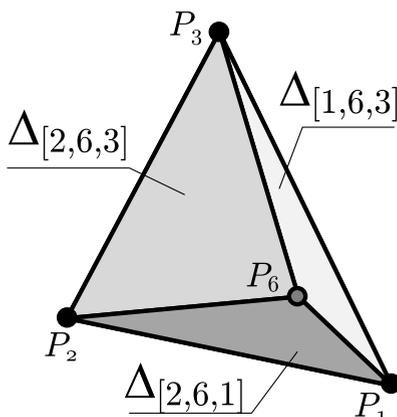
FIGURE 12. The general triangles arrangement for the proposed PWM duty cycle computation.

field term, corresponded to arbitrary input vectors arrangement [39]. The barycentric coordinate values for more complex analytical vector collections can be calculated using the Wachspress function. This issue has been discussed in the next subsection.

B. THE PWM DUTY CYCLES COMPUTATION CONCEPT FOR MULTIPHASE SYSTEMS

Electrical AC machines, generators, and voltage sources are described usually by a collection of voltage vectors. A presentation of AC voltages as a collection of rotating vectors using the analytical signal concept has been proposed in section I. Due to this concept, each voltage vector of the multiphase system can be represented exactly by one vector in cartesian coordinate space, as shown in Fig. 13. Theoretically, the rotation and pulsation of a given vector can be variable. Practically, the set of rotating vectors represents an electrical motor or generator voltages, which are symmetrical, regular and have one nominal frequency.
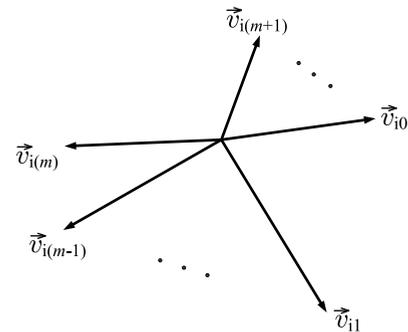
FIGURE 13. An analytic input vectors arrangement of the multiphase system.

The matrix converter topology permits for the time-proportioning output voltage synthesis, which means, that the desired output voltage is synthesized involving a certain number of the input voltages. We can use at least three selected vectors for this purpose or try to realize the synthesis based on the variable count of candidates. However, the physical restrictions and the principle of the vector projection method limit the modulation capabilities, which can be graphically represented by the synthesis field shown in Fig. 14. Theoretically, any convex polygon can be the synthesis field. However, regular and symmetrical polygons occur most frequently in practice. The regular type of vector arrangement can be assumed and considered for typical multiphase transformers and electrical machines [29].

The synthesis field can be constructed using any selected vector collection. Example variations of the synthesis field are illustrated in Fig. 15. The well–know the Three Nearest Vector Modulation scheme should be firstly considered because this solution is characterized by a relatively small switching number, good performance, and low output voltage THD. Generally, the synthesis field can form a different figure than the triangle. Such a scenario can take place during

the failure of one phase of the multiphase voltage source when the output voltage generation has to be maintained despite the mentioned problem. For instance, the five–phase induction machine can work with one supply phase that is broken [28]. Note, that the final properties of the chosen modulation scheme also depend on the switching sequence and commutation strategy [16], [40].

As reported earlier in the Introduction section, the calculation of the PWM duty cycles is pretty complicated in the case of the irregular shape of the synthesis field or the number of input voltage is greater than the typical value, which is equal to three [33]. The smooth interpolation technique can be used to solve this problem.

Let's assume, that a point P_o, with coordinates v_{ox} and v_{oy}, represents the analytic output voltage resides inside the synthesis field shown in Fig. 14. The PWM duty cycles for N number of input voltages, can be calculated using Wachspress formula for each input voltage $\vec{v}_{i0} \ldots \vec{v}_{i(m+1)}$ as follows

$$d\left(P_{(m)}\right) = \frac{w_{m(P_o, P_m)}}{\sum\limits_{k=1}^{N} w_{k(P_o, P_k)}} \tag{23}$$

where the numerator is the weight calculated as follows

$$w_{m(P_o, P_m)} = \frac{\Delta[m-1, m, m+1]}{\Delta[m-1, m, P_o] \cdot \Delta[P_o, m, m+1]} \tag{24}$$

According to the Wachspress approach properties [39], [41], the sum of all calculated duty cycles are equal unity

$$\sum_{k=1}^{N} d(P_k) = 1 \tag{25}$$

and in particular,

$$d(P_m) = 1 \Leftrightarrow P_m = P_o \tag{26}$$

Then conditions expressed by equations (2) and (3) are satisfied. Barycentric coordinates allow performing the voltage synthesis for any number of chosen input voltage greater equal three. Thus, various synthesis fields can be chosen.
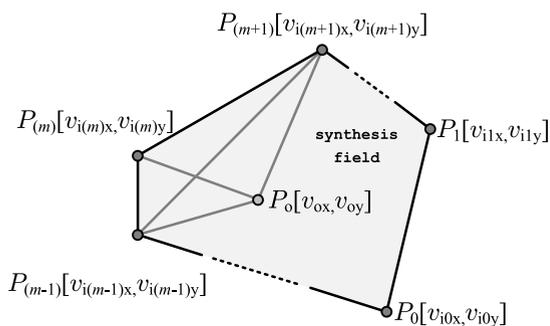
FIGURE 14. The synthesis field of the multiphase system.

The shape of the synthesis field changes in time because vectors are rotating. Therefore, the precision of the proposed synthesis scheme depends on the quadrature component
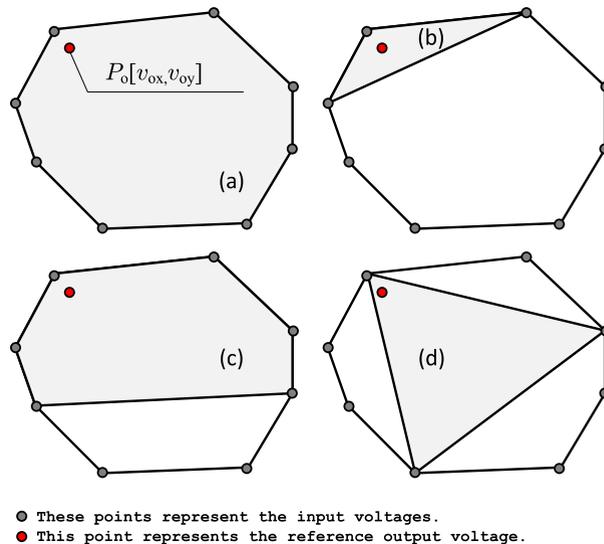
● These points represent the input voltages.
● This point represents the reference output voltage.

FIGURE 15. Example variations of synthesis field obtained for: (a) all vectors, (b) nearest three vectors, (c) selected arbitrarily, (d) three vectors selected arbitrarily.
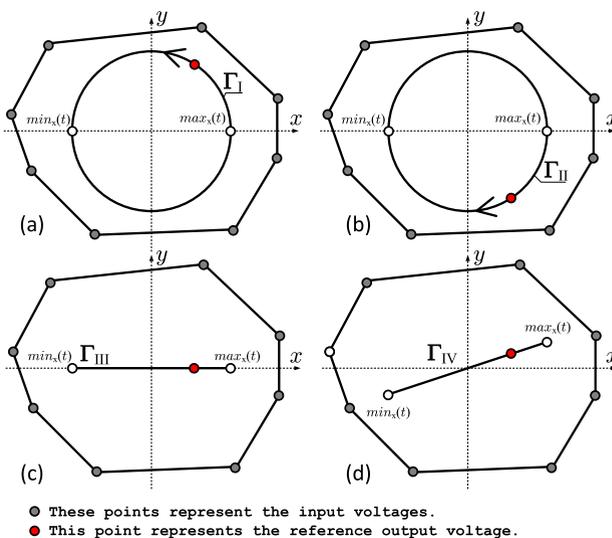
● These points represent the input voltages.
● This point represents the reference output voltage.

FIGURE 16. Example variations of centered trajectory: (a) rotation left, circular trajectory Γ_I, (b) rotation right, circular trajectory Γ_{II}, (c) the straight–line type of trajectory Γ_{III}, (d) modified rotated trajectory Γ_{IV} by straight sloping.

extraction algorithm [37]. The reference output voltage, which strictly corresponds to the x coordinates of the analytical output voltage, can be obtained by using a proper modulating signal. That signal can be represented by the *trajectory*, which is shown in Fig. 16, where four types of centered trajectory have been illustrated. Let's note, that the range of the real part of the modulating signal can be the same for all cases, thus the average output voltage is not affected by the y coordinates. Similar considerations are presented in publication [31]. A detailed analysis of the proposed approach has been presented in the next section.

IV. COMPREHENSIVE THEORETICAL ANALYSIS OF DIRECT MODULATION FOR CMC3 × 3 AND CMC3 × N

This section illustrates the problem of direct voltage modulation for a conventional matrix converter with three inputs and outputs. The analysis is divided into three parts. One selected case of the trajectory type has been discussed in subsections – a circular type of trajectory, straight–line type of trajectory, and optimal modified straight–line type of trajectory respectively. These types of trajectories shown in Fig. 16 in the previous section. Two major aspects have been taken into account – the characteristic of the input current for a given trajectory type and the available range of voltage transfer ratio.

The fundamental relations between the input and output voltages and currents can be written by two main equations. The first equation defines a relation between voltages

$$\mathbf{v}_o = \mathbf{v}_i \cdot \mathbf{D} \tag{27}$$

where output voltages are represented by

$$\mathbf{v}_o = \begin{bmatrix} v_{o1x} \\ v_{o2x} \\ v_{o3x} \end{bmatrix}^T = \begin{bmatrix} \mathrm{Re}\,(\bar{v}_{o1}) \\ \mathrm{Re}\,(\bar{v}_{o2}) \\ \mathrm{Re}\,(\bar{v}_{o3}) \end{bmatrix}^T \tag{28}$$

while input voltages are expressed as

$$\mathbf{v}_i = \begin{bmatrix} v_{i1x} \\ v_{i2x} \\ v_{i3x} \end{bmatrix}^T = \begin{bmatrix} \mathrm{Re}\,(\bar{v}_{i1}) \\ \mathrm{Re}\,(\bar{v}_{i2}) \\ \mathrm{Re}\,(\bar{v}_{i3}) \end{bmatrix}^T \tag{29}$$

and $\mathbf{D}$ contains required PWM duty cycles.

$$\mathbf{D} = \begin{bmatrix} d_{11} & d_{12} & d_{13} \\ d_{21} & d_{22} & d_{23} \\ d_{31} & d_{32} & d_{33} \end{bmatrix} \tag{30}$$

All elements d_{11}–d_{33} of the square matrix $\mathbf{D}$ can be calculated using proposed equations (19)–(22).

Let's note, that according to the proposed approach an analytic form is used to express input and output voltages in equations (28) and (29). By definition and nature of Hilbert's pair, only the measurable real part of these voltages physically exists. However, by entering the *imaginary* part of these signals, which has been explained in section II, the problem of PWM duty cycle computation has been resolved graphically based on barycentric coordinates.

The first column of the matrix $\mathbf{D}$ corresponds to the first input phase commutation group. There are three commutation groups in CMC3 × 3. By definition expressed by (2), the sum of the column elements must be equal to unity. In practice, the commutation issue can be developed and performed accordingly to the modulation schemes proposed in [40]. Among them, the Cyclic Venturini and MMM schemes of modulation have been described. Both fundamental equations have been proposed for the average–value model, in which the output voltage and input current are filtered by an ideal low pass filter. The higher–order harmonic analysis has been omitted here and further consideration has been focused on the average values only.

The input voltages from (12) for $V = 1$ can be represented by the normalized analytic voltage

$$\mathbf{v}_i = \begin{bmatrix} e^{j\omega_i} & e^{j\left(\omega_i - \frac{2\pi}{3}\right)} & e^{j\left(\omega_i + \frac{2\pi}{3}\right)} \end{bmatrix} \tag{31}$$

and the synthesis field, shown in Fig. 12 and Fig. 15(a). It can be graphically illustrated as an equilateral triangle. The collections of required triangle vertex coordinates can be obtained directly

$$\begin{aligned} \mathbf{v}_{ix} &= \mathrm{Re}\,(\mathbf{v}_i) \\ \mathbf{v}_{iy} &= \mathrm{Im}\,(\mathbf{v}_i) \end{aligned} \tag{32}$$

An important feature of the proposed approach is the ability of the modifying of the *imaginary* part of the modulating signals. Selected variations of the modulationg signal have been illustrated in Fig. 16 in the form of trajectories Γ_I–Γ_{IV}. The four principal cases of the reference analytic voltage formulas can be considered:

- circular type of trajectory with clockwise rotation

$$\bar{\mathbf{v}}_o(\Gamma_I) = q \cdot \begin{bmatrix} e^{j\omega_o t} \\ e^{j\left(\omega_o t - \frac{2\pi}{3}\right)} \\ e^{j\left(\omega_o t + \frac{2\pi}{3}\right)} \end{bmatrix}^T \tag{33}$$

- circular type of trajectory with clock–counter wise rotation

$$\bar{\mathbf{v}}_o(\Gamma_{II}) = q \cdot \begin{bmatrix} e^{-j\omega_o t} \\ e^{-j\left(\omega_o t - \frac{2\pi}{3}\right)} \\ e^{-j\left(\omega_o t + \frac{2\pi}{3}\right)} \end{bmatrix}^T \tag{34}$$
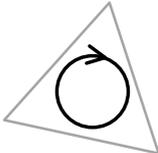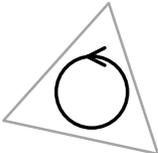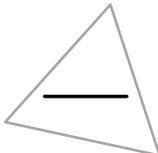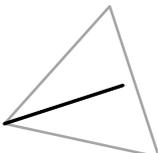
- straight–line type of trajectory

$$\bar{\mathbf{v}}_o(\Gamma_{III}) = q \cdot \begin{bmatrix} \cos(\omega_o t) \\ \cos\left(\omega_o t - \frac{2\pi}{3}\right) \\ \cos\left(\omega_o t + \frac{2\pi}{3}\right) \end{bmatrix}^T \tag{35}$$

- modified straight–line type trajectory by the rotation represented by the angle ϕ_i

$$\bar{\mathbf{v}}_o(\Gamma_{IV}) = q \cdot (1 + j\tan(\phi_i)) \cdot \begin{bmatrix} \cos(\omega_o t) \\ \cos\left(\omega_o t - \frac{2\pi}{3}\right) \\ \cos\left(\omega_o t + \frac{2\pi}{3}\right) \end{bmatrix}^T \tag{36}$$

Now, having both, the input and the output coordinate collections, each element of matrix $\mathbf{D}$ (30) can be elaborated using proposed formulas (19)–(22). Due to the complexity of the mathematical operation, the Matlab Symbolic Math Toolbox was used for support and verification. Results were additionally verified by a study based on PSIM11 simulation software. A detailed analysis can be performed using the script from Appendix 1. The script corresponds to the first case of the trajectory type. The analysis of the rest types of trajectories can be obtained by script row 18–20 modifications.

TABLE 1. Characteristics of the modulation for the example trajectory types for CMC3 × 3.

trajectory	maximum voltage transfer ratio q_{max}, input angle ϕ_i, and $\alpha\beta$ average input currents
	$q_{max} = 0.5$ $\phi_i = +\varphi_o$ $i_{i\alpha} = q \cdot I_{o\,max} \cdot \cos(\omega_i t + \varphi_o)$ $i_{i\beta} = q \cdot I_{o\,max} \cdot \sin(\omega_i t + \varphi_o)$
	$q_{max} = 0.5$ $\phi_i = -\varphi_o$ $i_{i\alpha} = q \cdot I_{o\,max} \cdot \cos(\omega_i t - \varphi_o)$ $i_{i\beta} = q \cdot I_{o\,max} \cdot \sin(\omega_i t - \varphi_o)$
	$q_{max} = \frac{1}{\sqrt{3}}$ $\phi_i = 0$ $i_{i\alpha} = q \cdot I_{o\,max} \cdot \cos(\varphi_o) \cdot \cos(\omega_i t)$ $i_{i\beta} = q \cdot I_{o\,max} \cdot \cos(\varphi_o) \cdot \sin(\omega_i t)$
	$q_{max} = \frac{\sqrt{3}\cdot\cos(\phi_i)}{2}$ $\phi_i \in \left(-\frac{\pi}{2}, \frac{\pi}{2}\right)$ $I_o = q \cdot I_{o\,max} \cdot \cos(\varphi_o)$ $i_{i\alpha} = I_o \cdot (\cos(\omega_i t) - \tan(\phi_i) \cdot \sin(\omega_i t))$ $i_{i\beta} = I_o \cdot (\sin(\omega_i t) + \tan(\phi_i) \cdot \cos(\omega_i t))$

The second important formula describes the relationship between the input and output currents as follows

$$\mathbf{i}_i = \mathbf{i}_o \cdot \mathbf{D}^T \qquad (37)$$

The average input currents can be calculated using the matrix $\mathbf{D}$ transposition. Again, the proposed script can be used for finding theoretical formulas and analysis purposes. This research performed under assumption of sinusoidal output voltage and linear *RL* load with load angle φ_o. Analysis results are collected and presented in Table 1. The first two cases, which are characterized in Table 1, allow regulating the input angle without the voltage transfer ratio value decrease. These modulation schemes can be classified as the Venturini approach. The last two trajectories represent more practical importance because the maximum voltage transfer ratio q_{max} is greater than 0.5. Let's see again the trajectory illustrations shown in Fig. 16. The distance between points marked as min_x and max_x denote peak–to–peak line–to–line voltage in the linear range of modulation. An increasing voltage transfer ratio can be performed by adding the common–mode signal to the modulating signal. Thus, the maximum length of the trajectory can reach the 3/4 of the value. The whole trajectory must lie inside the synthesis field according to the proposed

voltage synthesis concept, therefore the appropriate trajectory position has to be calculated and changed all the time.

The changes in the trajectory position can be controlled by the displacement vector. The exemplary cases are presented in Fig. 17. In all cases, the trajectory lies inside the synthesis field, which instantaneously rotating. The length of trajectory, in the meaning of the distance between the minimal and maximal instantaneous output voltages also changes in time. If the certain output voltage overlaps with the one of the input voltage, as shown in Fig. 17(a) and (d), the commutation group will not switching. Thus theoretically, by using such a strategy, the total number of switching can be reduced.
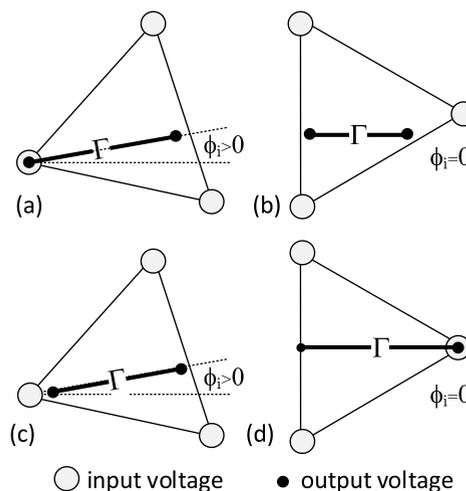

FIGURE 17. The position of the trajectory inside the synthesis field: (a) the one output minimal voltage overlaps the one input voltage, (b) arbitrarily location, (c) rotated trajectory but none points overlap, (d) the trajectory has a maximum length and is tied with one of the triangle vertices.

Considering the *n*–number of output phases of the matrix converter supplied by the three–phase source, the following conclusion can be formulated. Using the modulation technique with the common mode signal injection, defined as

$$v_{cm} = -0.5(max_x + min_x)$$
$$max_x = \text{MAX}\{v_{o1x}, v_{o2x}, ..., v_{onx}\}$$
$$min_x = \text{MIN}\{v_{o1x}, v_{o2x}, ..., v_{onx}\} \qquad (38)$$

the maximum value of voltage transfer ratio q for *n*–phase topology and angle $\phi_i = 0$, can be expressed as follows

$$q_{max}(n) = \begin{cases} 0.75 & \Leftrightarrow n \in \{4, 6, 8, ...\} \\ 0.75/\cos(\pi/(2n)) & \Leftrightarrow n \in \{3, 5, 7, ...\} \end{cases} \qquad (39)$$

Considering non–zero ϕ_i value, the following final formula for maximum voltage transfer ratio can be proposed

$$q_{max}(n, \phi_i) = q_{max}(n)\cos(\phi_i) \qquad (40)$$

Finally, the following modulating signal can be selected for further investigation as an optimal

$$\bar{\mathbf{v}}_o = (\mathbf{v}_o + v_{cm}) \cdot \begin{bmatrix} 1 & \tan(\phi_i) \end{bmatrix} \qquad (41)$$
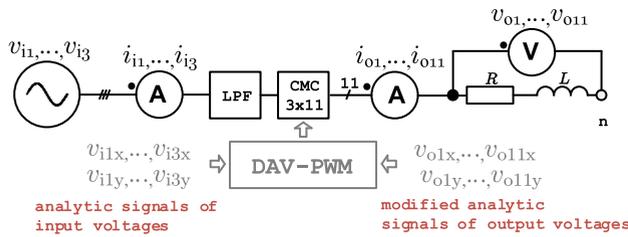
FIGURE 18. A simplified circuit configuration of CMC3 × 11 converter used in the simulation research.

A practical implementation details, including the algorithm flow chart for CMC3 × N, commutation strategy, and PWM modulation scheme under abnormal input conditions, have been presented in the separate open access paper [37] as the Direct Analytic Vector PWM (DAV–PWM) modulation.

The proposed approach of the PWM duty cycle computation in the direct modulation for the matrix converter has been verified and validated using the PSIM simulation software. The selected results were graphically processed in Matlab and Visio programs. In most cases, the value of the waveform has been presented using p.u. units based on RL–type load. The control board has been modeled using the general DLL block and discrete numerical step equal to the 0.2 ns. The C–code corresponded to the proposed algorithm was called and performed every 100 μs. All required signals from the simulation scheme and control path were connected to inputs and outputs of the DLL block.

A. MATRIX CONVERTER WITH 3 INPUTS AND 11 OUTPUTS
By employing a higher number of electrical motor phases the torque ripples can be reduced. Moreover, in such drives, the current load per phase is decreased. This ensures satisfactory performance of the mechanical system of the inverter–fed motor even at lower speed. It has also been established that the electrical efficiency of the inverter–fed multiphase motors is higher. Increasing the phase numbers will also improve reliability since the drive can start and run even after stator phase failure [28], [29]. The proposed calculation scheme for the 11–phase RL type load, based on the analytical signal concept, has been successfully verified during the simulation research. A simplified simulation circuit configuration with the CMC3 × 11 converter is shown in Fig. 18. All required PWM duty cycles have been calculated using the DAV–PWM modulation method described in [37]. The Min–Mid–Max (MMM) switching strategy presented in [40] has been adopted. As can be observed in Fig. 19, the *real*, *x* part of the line–to–line analytical voltage is sinusoidal and the load current $i_{o1}, ..., i_{o11}$ are generated properly. The waveforms are shown in Fig. 19 were obtained for the following circuit and control parameters: $\phi_i = 0$, $\omega_i = 2\omega_o$, $q = q_{max} = 0.757$, $R = 0.5\Omega$, and $L = 8.3\ mH$.

A large number of output phases doesn't make a significant complexity at all. The PWM duty cycle computation scheme is the same for all output voltages. Therefore the optimized pipelined DSP operations can be used to reduce the runtime. Further development can be performed using FPGA devices.

Digital configurable structures are very convenient for hardware designers because them offer a great feature of code execution acceleration.

B. AN INPUT ANGLE CONTROL
Fully independent control of the input power factor, in a matrix converter, is not available because of the fundamental relation between the input and output voltages (27) and currents (37). Nevertheless, when the matrix converter does not operate with its own maximum transfer ratio (it means the maximum length of the reference output voltage trajectory inside the synthesis field), an input angle can be set to achieve a desired input power factor. The proposed algorithm of power factor regulation has been verified for CMC3 × 5 converter, where analytical considerations have been also confirmed. The example results, for three values of ϕ_i, are shown in Fig. 20 and Fig. 21 respectively. Waveforms were obtained for the following circuit and control parameters: $\omega_i = 2\omega_o$, $q = \cos(\pi/6)(0.75/\cos(\pi/10))$, $\omega_i = 2\omega_o$, $R = 0.53\Omega$, and $L = 5.3\ mH$.

The maximum voltage transfer ratio q is dependent on the cosine of angle ϕ_i, thus to maintain the constant amplitude of the sinusoidal output current, an appropriate value of q should be set.

The regulation of an input angle is realized in a simple way using the formula (41) by the modification of the trajectory position inside the synthesis field. Such a method can be used for any number of output phases.

The line–to–line analytical voltage waveform, represented by difference $v_{o1x} - v_{o2x}$, remains unchanged. Thus, the output current waveforms, $i_{o1}, ..., i_{o5}$, are independent of an input angle ϕ_i regulation.

C. ASYMMETRY OF THE INPUT VOLTAGES
AC output voltages are generated using the AC input voltages. It is a general rule of direct voltage synthesis [1], [3]. If the input voltages are not purely sinusoidal than the output voltage can be deformed. It strongly depends on the applying approach to CMC control. The paper propose the direct method variant, which can be compared to the scalar or Venturini methods. Such a comparison has been presented in [37].

Applying the formula (13) to voltages that are slightly deformed, in particular asymmetrical, leads to the input current distortion. Nevertheless, as shown in Fig. 22, the shape of the output current is still pure sinusoidal despite the 20% asymmetry of the first source phase. The advanced method of analytic signal generation, discussed in section I, can be used to improve the shape of the average (filtered) input currents. Compare to the basic version of the Hilbert pairs generation, an advanced Hibert transform presents better input current quality.

D. THE GRID VOLTAGE WITH HIGHER–ORDER HARMONICS
The shape of the synthesis field is strongly dependent on the effect of input voltage harmonic analysis. The precise
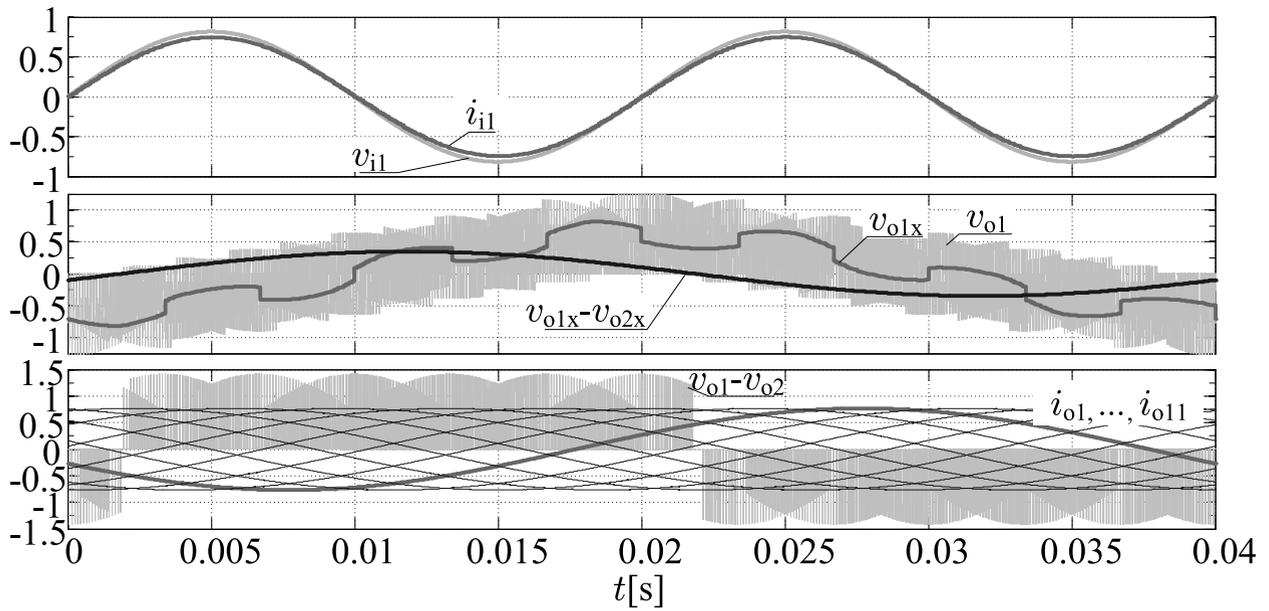
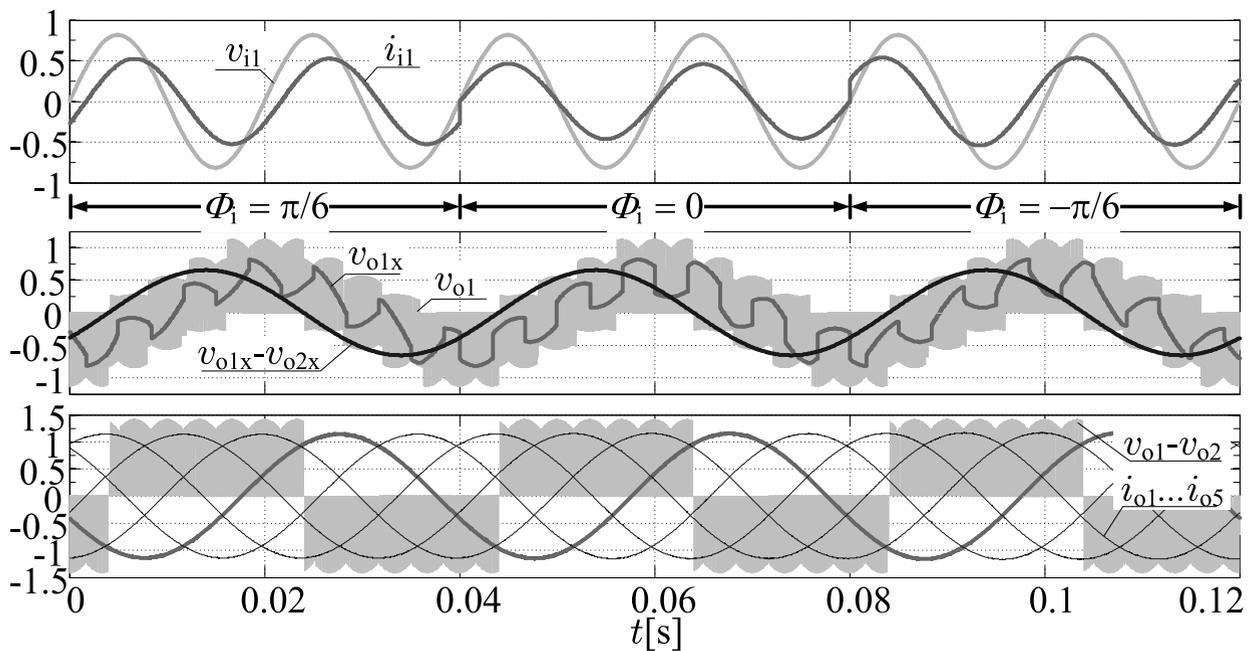**FIGURE 19.** The control of CMC3 × 11 converter under unity power factor operation.

FIGURE 20. Power factor regulation in CMC3 × 5 converter for $\phi_i = \{\pi/6, 0, -\pi/6\}$.

detection of harmonic and an analytic signal generation [34], [35], [42], [43] permit for controlling the input angle and generate the proper load voltages. An example waveforms have been shown in Fig. 23. Presented results have been obtained under the assumption of the known spectrum of the higher-order harmonics. Considering formal compatibility with theoretical Hilbert transform, usage of the equation (13) is limited to the balanced sinusoidal source. Nevertheless, if the application only concentrates on the sinusoidal shape of the load current, this simple formula may be applicable

for various shape voltage waveforms, as shown in Fig. 24. A proposed approach has been verified also experimentally. The basic tests have been performed for CMC3 × 3 and balanced sinusoidal source. A comparison of the simulation and experimental results has been shown in the next subsection.

The presented simulation results are promising. Nevertheless, it should be remembered, that in practical conditions, accurate harmonic analysis generates the computation delay and achieving good performance of the control is obtained only for accurately determined signals.
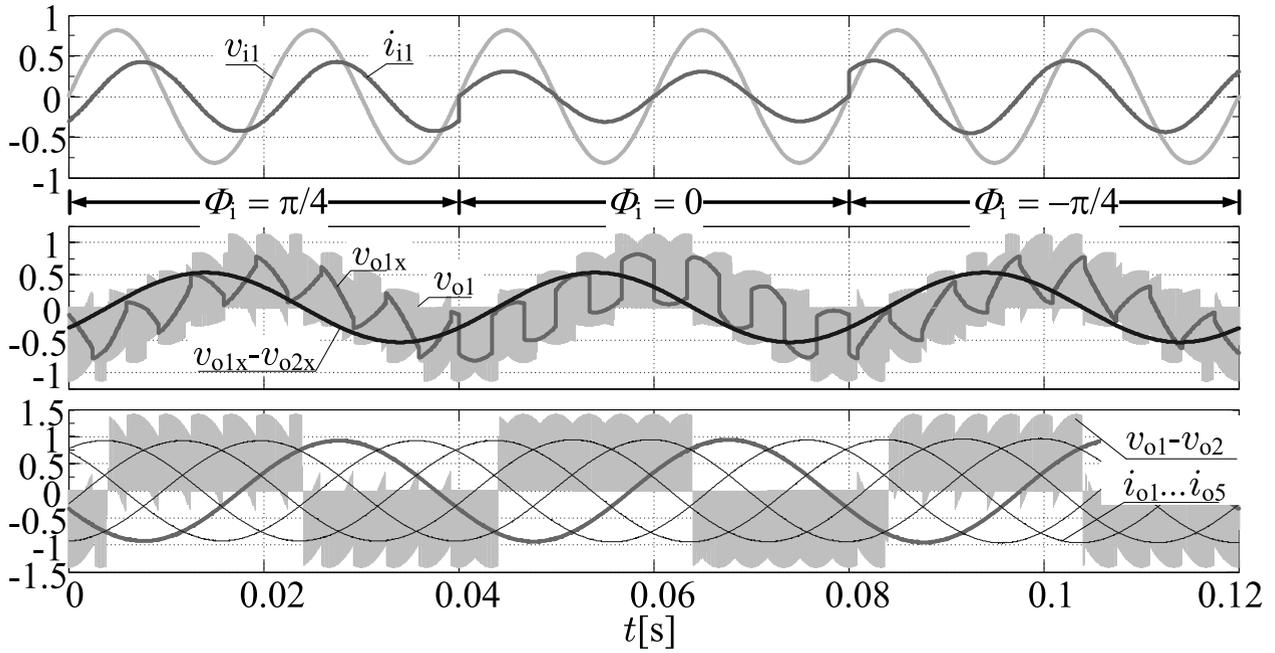
FIGURE 21. Power factor regulation in CMC3 × 5 converter for $\phi_i = \{\pi/4, 0, -\pi/4\}$.
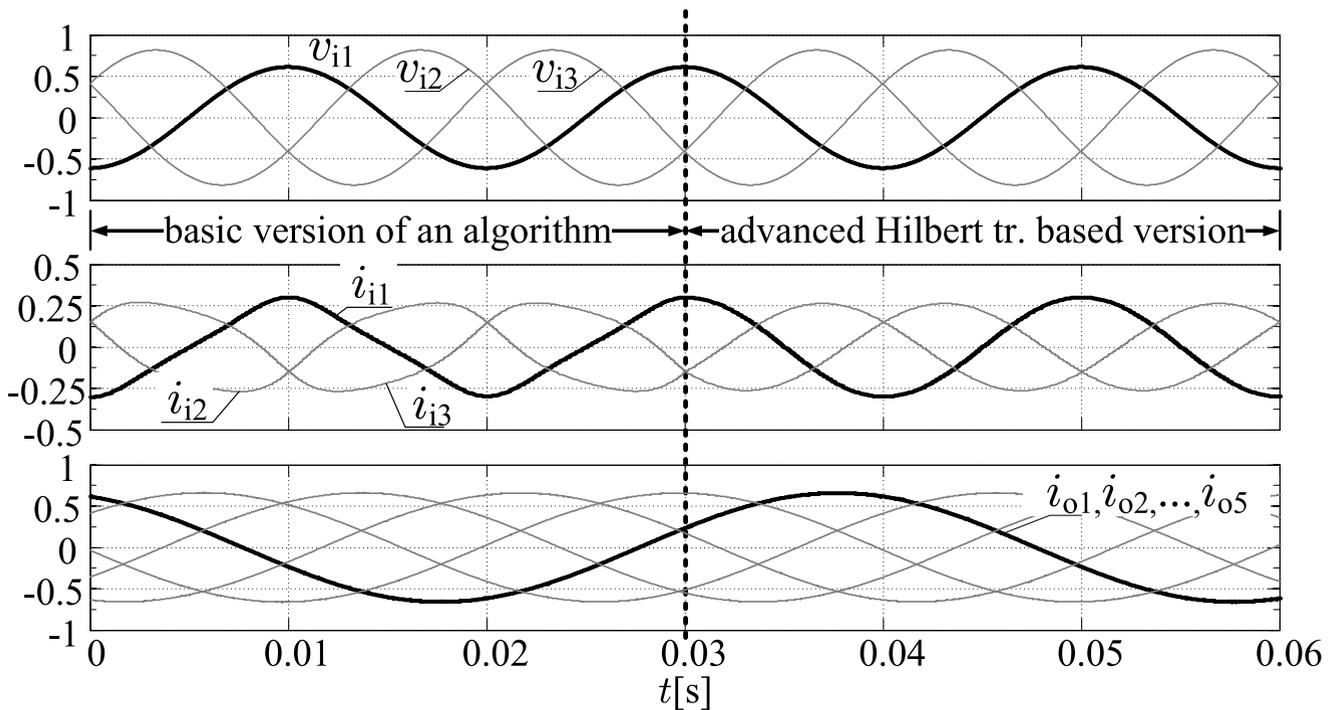

FIGURE 22. An input current waveform comparison, in CMC3 × 5 converter, for the basic and advanced version of the Hilbert transform.

The proposed method, in the context of the results presented in Fig. 23 and Fig. 24, was not tested experimentally due to the lack of appropriate equipment. Such work is planned to be carried out in the future. However, the possibility of immediate switching of various types of power supply with maintaining a sine wave output current seems to be very perspective.

E. COMPARISON OF THE SIMULATION AND EXPERIMENTAL RESULTS FOR CMC3X3

The proposed novel approach for CMC3 × 3 has been verified in the laboratory using a prototype converter. Fig. 25 illustrates the CMC prototype and control board photos. The proposed algorithm has been implemented with floating–point multicore digital signal processor Analog Devices
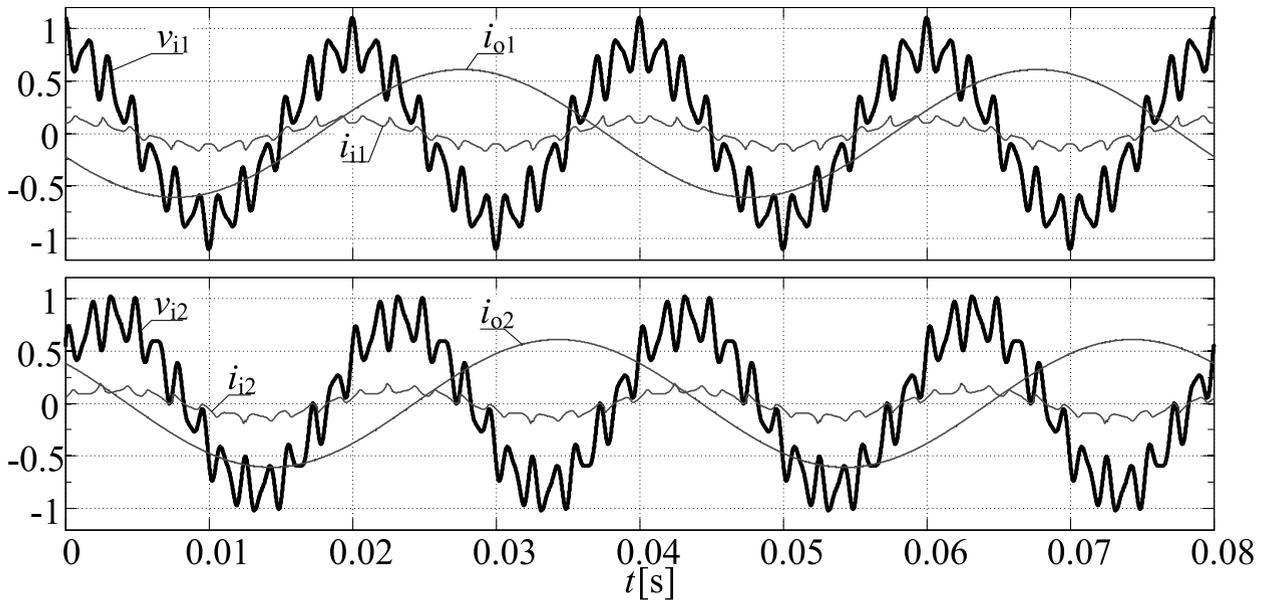
FIGURE 23. The synthesis of the pure sinusoidal output currents in CMC3 × 5 under abnormal input conditions in the form of high–order harmonic distortion: $\omega_i = 2\omega_o$.
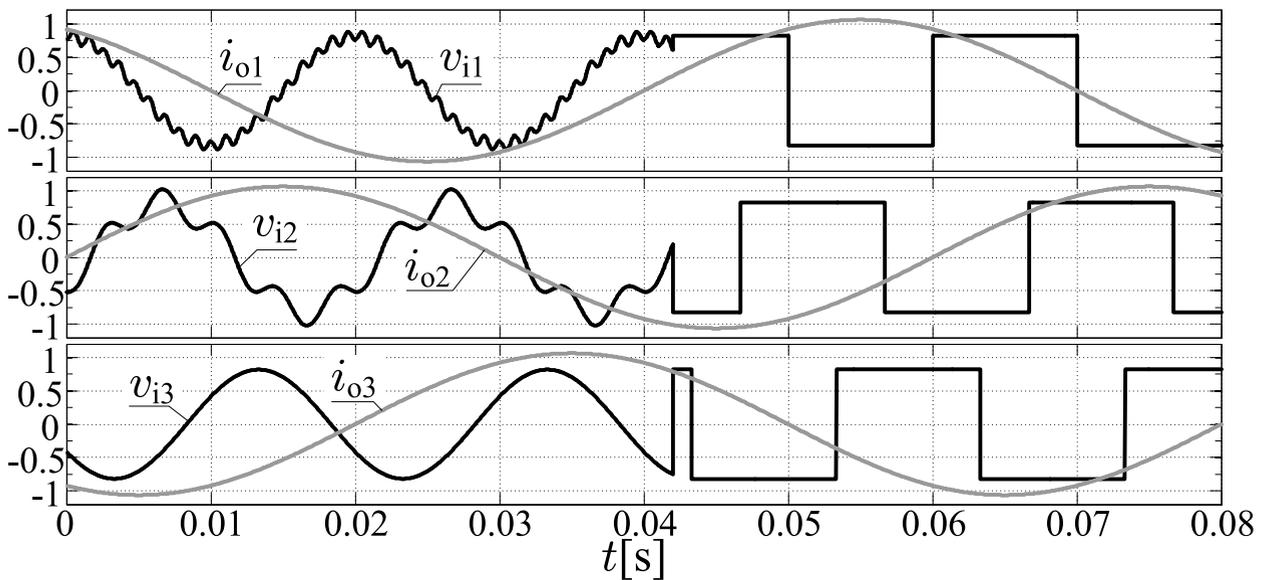

FIGURE 24. An effect of proper output voltage synthesis for the three non–sinusoidal input voltages: $\omega_i = 3\omega_o$.

ADSP–SC589. A programmable logic device Intel FPGA MAX10 has been used mainly for performing a four–step commutation and analog–to–digital acquisition. System commands have been served by the user console software connected with the control board via fiber optic. Most important setup parameters are collected in Table 2. The description of markings used in figures is listed in Table 3.

Results presented in Fig. 26 to Fig. 29 demonstrate quite good theoretical–practical coherence of the proposed solution and, in particular, the proper generating of the load current. However, an input angle control has been performed in open–loop mode only without consideration of the displacement generated by the input capacitor filter. Moreover, the paper focuses on a novel PWM duty cycle computation

and the higher-order harmonic analysis has been omitted here. Note, that the Cyclic–Venturini switching approach was adopted [40]. The proposed method rather belongs to the scalar method, in which the switch operation time is obtained directly. Theoretically, the switching sequence can be developed in many ways: Cyclic Venturini method, MMM method, discontinuous modulation, etc.

V. DIRECT MODULATION SCHEMES FOR MULTIPHASE CONVENTIONAL MATRIX CONVERTERS WITH FIVE INPUTS

The multiphase motor drives applications require a voltage converter with more than three outputs. These applications offer an inherent advantage compared to their three–phase

TABLE 2. Parameters of the laboratory setup.

Parameter	Value
Source line–to-line voltage	$V_i = 100V$
	fed by a step–down transformer
Input frequency	$f_i = 50Hz$
Input filter	$C_f = 15\mu F$, $L_f = 200\mu H$
Cabling resistance	$R_f = 0.1\Omega$
Switching frequency	$f_s = 10kHz$
Three–phase load	$R = 30\Omega$, $L = 9mH$
Operating power	5kVA

TABLE 3. Description of markings in Figures 26, 28, 27, 29.

$v_{o1,2}$	line–to–line load voltage
i_{o1}	load current
v_{i1}	grid voltage
i_{i1}	grid current
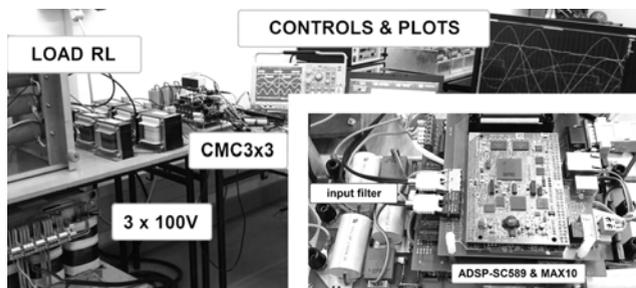
FIGURE 25. Photos of an experimental setup.

experiment

simulation

FIGURE 26. Unity input power factor operation of the matrix converter, comparison of experiment and simulations results for CMC3 × 3: $q = 0.86$, $\omega_i = 2\omega_o$, $\phi_i = 0$.
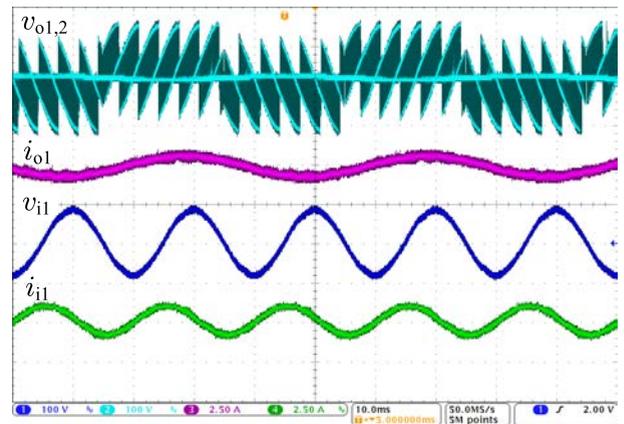
FIGURE 27. Operation of matrix converter with reference input angle $\phi_i = \pi/3$, experimental results for CMC3 × 3: $q = 0.8 \cos(\phi_i)$, $\omega_i = 2\omega_o$.

counterparts, such as higher efficiency, lower torq ripple, and increased reliability [28], [29], [44]. Multiphase electric machines can be fed also by the conventional matrix converter with three inputs [19]–[21], [45]. The matrix topology is also presented as a unit, which control the power flow between the voltage generator and the supply grid [30], [46]–[49]. Multiphase generators have also been used in systems generating electricity such as offshore installations and wind farms [50], [51]. On the other hand, the power density can be increased using the high–speed multiphase generators. Although generators with the number of phases 6 and 9 are more applicable [44], [51], for simplicity of the consideration, a 5–phase generator connected with the 5-input matrix converter has been mainly presented.

This section addresses the issue of the problem of the PWM duty cycle computation for CMC5 × 3 and CMC5 × 5 converters connected with standard three–phase voltage grid through the grid LCL filter, shown in Fig. 30, or using the dedicated transformer [52]–[54]. The power flow is a task located in the higher layer of the overall control, thus this application aspect has been omitted here. The simplified circuit configuration with the special 5–to–3 transformer is shown in Fig. 31.

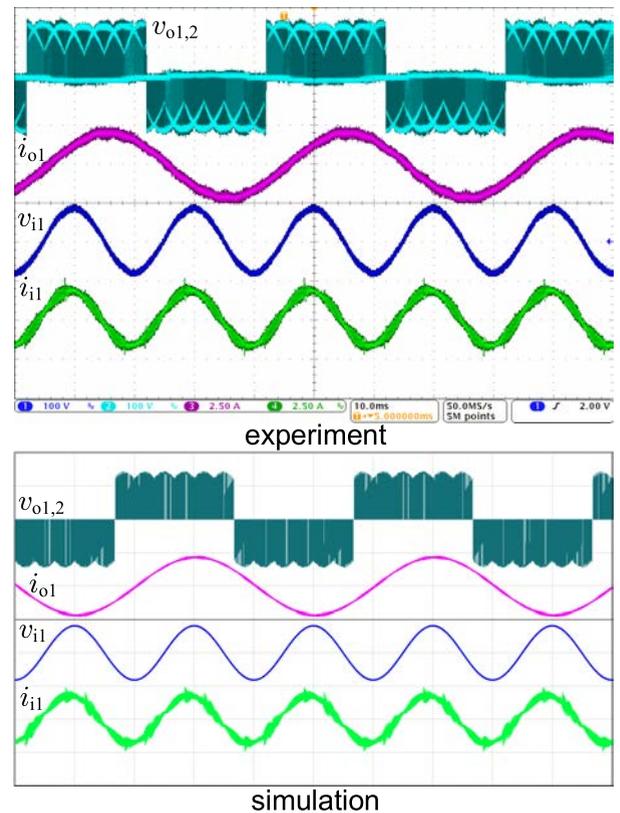Given the results discussed above the proposed approach is analogous and developed both using the analytical signals and barycentric coordinates concepts. At first lets assume, that the CMC is connected to the ideal five–phase voltage source represented by five rotating vectors. In this case, the synthesis field is a pentagon, which rotates with certain generator voltage pulsation. Two types of the modulating signal trajectory were considered: the straight–line (Fig. 32), and the circular trajectory (Fig. 33).
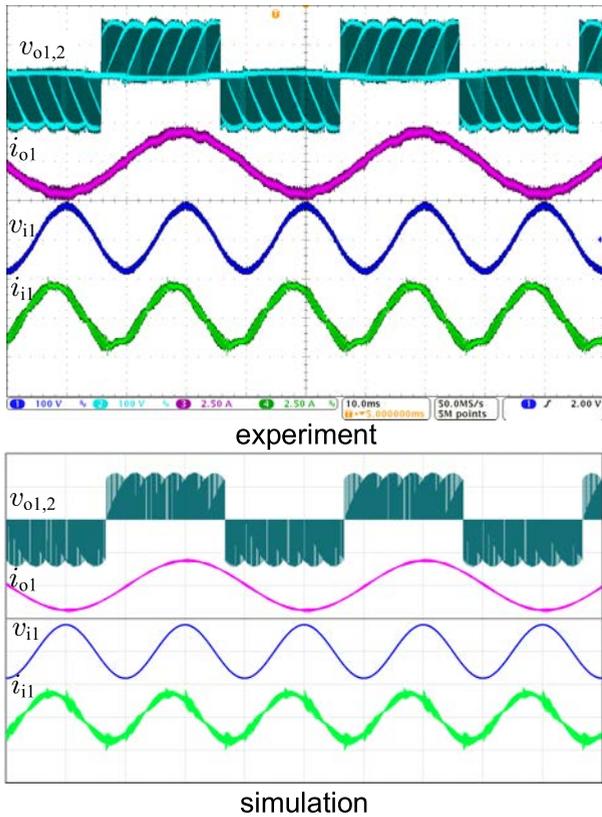
experiment

simulation

FIGURE 28. Operation of matrix converter with reference input angle $\phi_i = \pi/6$, comparison of experiment and simulations results for CMC3 × 3: $q = 0.8 \cos{(\phi_i)}$, $\omega_i = 2\omega_o$.

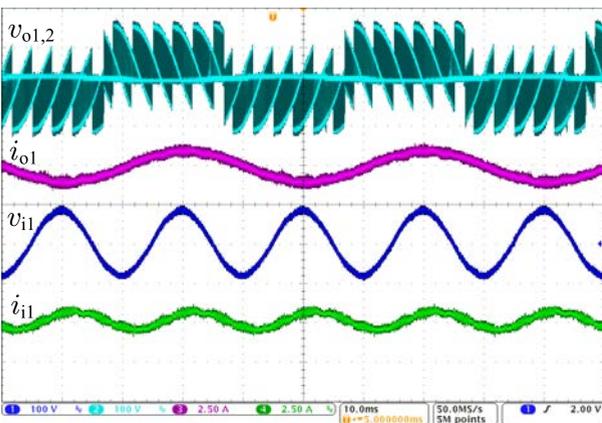**FIGURE 29.** Operation of matrix converter with reference input angle $\phi_i = -75\pi/180$, experimental results for CMC3 × 3: $q = 0.8 \cos{(\phi_i)}$, $\omega_i = 2\omega_o$.

The maximum value of the voltage transfer ratio for the circular trajectory can be expressed as follows

$$q_{\text{max}} = \cos\left(\frac{2\pi}{5} \cdot \frac{1}{2}\right) = 0.809 \qquad (42)$$

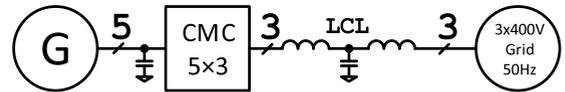for both converters – CMC5 × 3, and CMC5 × 5. By using the straight–line type of trajectory and common mode signal

FIGURE 30. Simplified energy conversion system with CMC5 × 3 and LCL grid filter.
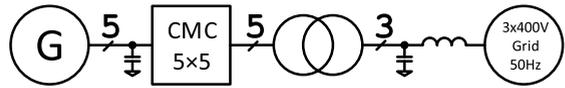
FIGURE 31. Simplified energy conversion system with CMC5 × 5 and special grid transformer.
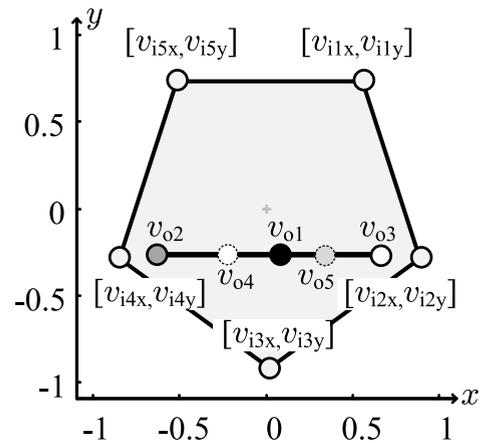
FIGURE 32. The straight–line trajectory of the modulating signal.
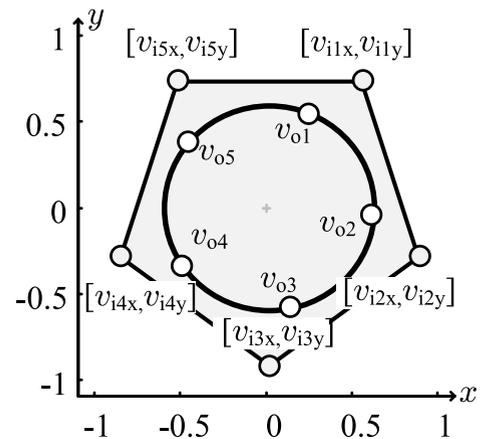
FIGURE 33. The circular trajectory of the modulating signal.

injection technique, the maximum voltage transfer ratio q_{max} can be increased to the value

$$q_{\text{max}} = \frac{1 + \cos\left(\frac{\pi}{5}\right)}{2 \cdot \cos\left(\frac{\pi}{2 \cdot 3}\right)} = 1.044 \qquad (43)$$

in the case of CMC5 × 3. For the CMC5 × 5 the maximum voltage transfer ratio can be calculated using a similar

FIGURE 34. The PWM duty cycles calculation for the reference output voltage, represented by point 6, using the Wachspress scheme of computing.

equation

$$q_{\max} = \frac{1 + \cos\left(\frac{\pi}{5}\right)}{2 \cdot \cos\left(\frac{\pi}{2 \cdot 5}\right)} = 0.9511 \qquad (44)$$

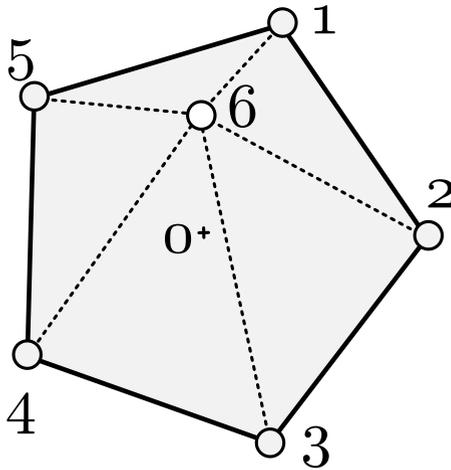Theoretically, an average output voltage can be generated using the freely selected input voltage collection. The PWM duty cycles for CMC3 $\times$ N can be computed by the smooth interpolation methods, which are transformed into the simple rational function of triangle areas. The solution for the multiphase system can also be constructed based on the analogous graphical–vector arrangement. According to the synthesis field concept, the Wachpress rational functions (23), permit for direct computation. A further consideration is focused on just the three graphical–vector arrangements. So, the three following calculation schemes can be proposed and analyzed:

- using the Wachspress barycentric coordinates for the pentagon,
- applying the virtual zero–component, the triangular input voltage sectors, and the rational function of triangle areas,
- adopting the Nearest Three Vectors approach and barycentric coordinates for the triangular synthesis field.

COMPUTATION OF THE PWM DUTY CYCLES USING THE WACHSPRESS BARYCENTRIC COORDINATES

If the synthesis field is a regular polygon, as shown in Fig. 34, the Wachspress formula (23), calculated for reference output voltage marked in the figure by point 6, can be simplified to the following expression

$$d_{16} = \frac{\Pi_{16}}{\Pi_{16} + \Pi_{26} + \Pi_{36} + \Pi_{46} + \Pi_{56}} \qquad (45)$$

where

$$\Pi_{16} = \Delta_{[6,2,3]} \cdot \Delta_{[6,3,4]} \cdot \Delta_{[6,4,5]}$$
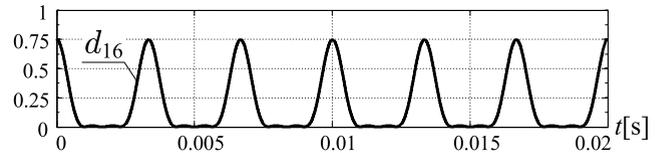$$\Pi_{26} = \Delta_{[6,3,4]} \cdot \Delta_{[6,4,5]} \cdot \Delta_{[6,5,1]}$$

FIGURE 35. The example waveform of PWM duty cycle d_{16} for the circular trajectory with clockwise rotation of the reference output vector: $q = 0.8$, $\omega_o = 5 \cdot \omega_i$, and $\omega_i = 2 \cdot \pi \cdot 50$.

$$\Pi_{36} = \Delta_{[6,4,5]} \cdot \Delta_{[6,5,1]} \cdot \Delta_{[6,1,2]}$$
$$\Pi_{46} = \Delta_{[6,5,1]} \cdot \Delta_{[6,1,2]} \cdot \Delta_{[6,2,3]}$$
$$\Pi_{56} = \Delta_{[6,1,2]} \cdot \Delta_{[6,2,3]} \cdot \Delta_{[6,3,4]} \qquad (46)$$

The $\Delta_{[i,j,k]}$ is an area of triangle with vertices i, j, and k respectively. The area is calculated using the determinant of a square matrix, which contains coordinates of analytical voltages, as presented in previous sections. All the rest PWM duty cycles, $d_{26} \cdots d_{56}$, are calculated by the same method. The example waveform of PWM duty cycle d_{16} for the presented method has been shown in Fig. 35. The Wachspress barycentric coordinates are also very useful for irregular polygons, which can represent the graphical–vector arrangements of asymmetrical AC voltages. All available vectors are involved in voltage synthesis, as well as the power switches. Thus, this solution is not optimized due to switching. However, the computation scheme is uniform and this solution can be applied for special cases, such as temporary amplitude or angle voltage asymmetry, rapidly source failure, etc.

COMPUTATION OF THE PWM DUTY CYCLES APPLYING THE VIRTUAL ZERO–COMPONENT AND THE TRIANGULAR INPUT VOLTAGE SECTORS

The symmetrical arrangement of the input vectors allows to define the virtual zero–component voltage represented by the point with coordinates indicating the midpoint of the pentagon. This voltage is represented by the point 0 in Fig. 36. The PWM duty cycles can be calculated for local triangular synthesis field with vertices 5, 1, and 0 as follows

$$d_5 = \frac{\Delta_{[6,1,0]}}{\Delta_{[5,1,0]}}$$
$$d_1 = \frac{\Delta_{[6,5,0]}}{\Delta_{[5,1,0]}}$$
$$d_0 = \frac{\Delta_{[6,5,1]}}{\Delta_{[5,1,0]}} \qquad (47)$$

Thus formally the synthesis of the v_{o6x} output voltage can be represented by the equation below

$$v_{o6x} = d_1 \cdot v_{i1x} + d_5 \cdot v_{i5x} + \frac{d_0 \cdot (v_{i1x} + v_{i2x} + v_{i3x} + v_{i4x} + v_{i5x})}{5} \qquad (48)$$

After grouping the PWM duty cycles in the above equation, the following formula is finally obtained
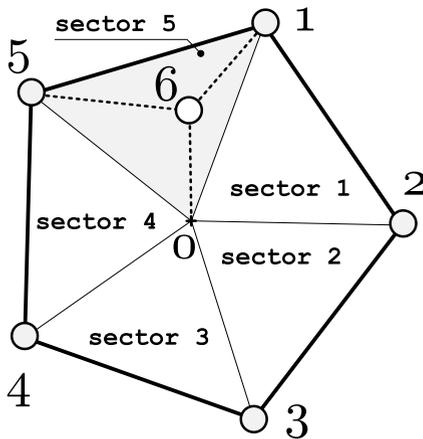
$$d_{56} = d_5 + \frac{d_0}{5}$$

FIGURE 36. The PWM duty cycles calculation for the reference output voltage, represented by point 6, using the Zero–Component Voltage and triangular sector.
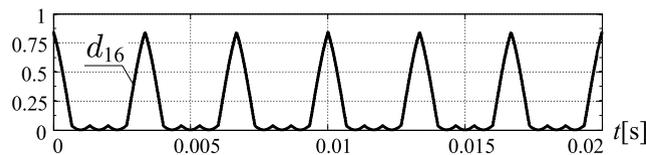

FIGURE 37. The example waveform of PWM duty cycle d_{16} for the circular trajectory with clockwise rotation of the reference output vector: $q = 0.8$, $\omega_o = 5 \cdot \omega_i$, and $\omega_i = 2 \cdot \pi \cdot 50$.

$$d_{16} = d_1 + \frac{d_0}{5}$$

$$d_{26} = d_{36} = d_{46} = \frac{d_0}{5} \qquad (49)$$

The proposed method can be used for a circular modulating signal. Operations realized in the other four triangular sections are performed in an analogous manner. Fig. 37 shows the example waveform of PWM duty cycle d_{16} for the discussed approach of calculation.

Subsection presents a less complicated solution compared to the previous approach. The computations are reduced to the direct relation of triangle areas. Such an approach can be applied for regular synthesis fields and symmetrical multiphase systems. The proposed concept is near to the classic view of modulation. However, high switching is still a disadvantage and the switching sequence optimization is preferable. A short–time vectors can be eliminated through the switching sequence or the switching sequence can be rearranged in the context of commutations.

A. COMPUTATION OF THE PWM DUTY CYCLES ADOPTING THE NEAREST THREE VECTORS APPROACH

In general, the nearest three vectors PWM (NTV–PWM) modulation is not complicated and allows to reduce the switching losses and improve the output voltage quality. As demonstrated in section II, the PWM duty cycles can be expressed by the triangles area ratio. Based on the triangle $\Delta_{[5,1,2]}$ illustrated in Fig. 38 the required PWM duty cycles
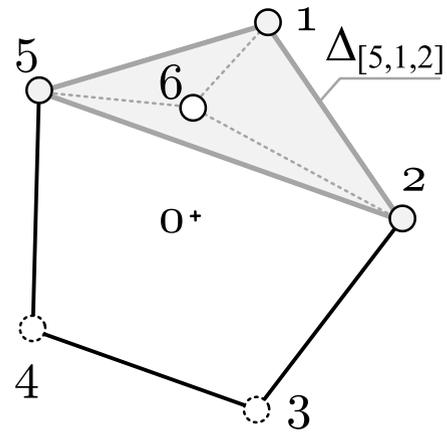

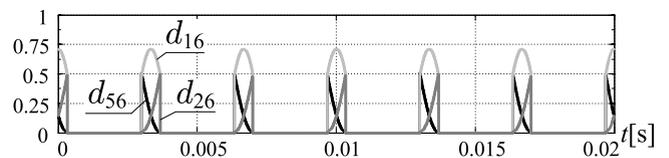**FIGURE 38.** Modulation scenario using only the nearest three vectors.

FIGURE 39. The example waveform of PWM duty cycle d_{16} for the circular trajectory with clockwise rotation of the reference output vector: $q = 0.8$, $\omega_o = 5 \cdot \omega_i$, and $\omega_i = 2 \cdot \pi \cdot 50$.

can be calculated using the following formulas

$$d_{56} = \frac{\Delta_{[6,1,2]}}{\Delta_{[5,1,2]}}$$

$$d_{16} = \frac{\Delta_{[6,2,5]}}{\Delta_{[5,1,2]}}$$

$$d_{26} = \frac{\Delta_{[6,5,1]}}{\Delta_{[5,1,2]}} \qquad (50)$$

The example waveform of PWM duty cycle d_{16}, d_{26}, and d_{56} have been shown in Fig. 39.

According to the proposed synthesis scheme, the reference output voltage represented by point 6 must lie inside the just formed triangle. The rest of the input vectors, which do not belong to the selected triangle, are not used during generation the given output voltage.

An example phase output voltage and load current waveforms of CMC5×5 for discussed methods of PWM duty cycle computing has shown in Fig. 40, where the symulation results have been only presented. A detailed higher–order harmonic analysis and comparison for these variants of modulations will be presented in a separate paper.

Table 4 presents a THD index for each modulation type shown in Fig. 40. These values have been calculated using the THD calc tool in PSIM11 simulation software. Based on the results obtained, it can be indicated that the latest modulation method has the best most–favorable THD coefficient. For the voltage transfer values, which are near to the maximal voltage gain, and the greater number of phases, the NTV modulation technique is the best choice due to low total harmonic distortion.
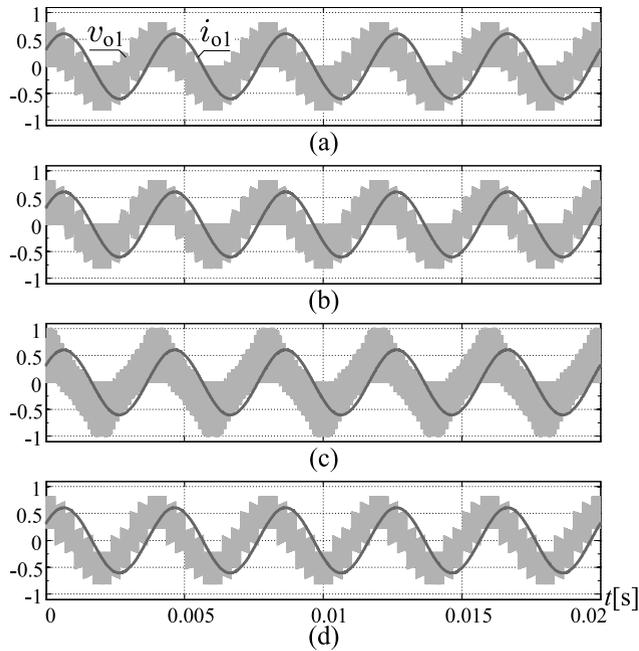
FIGURE 40. The comparison of the phase output voltage shape for different methods of PWM duty cycle computing for $q = 0.8$, $\phi_i = 0$, $\omega_o = 5 \cdot \omega_i$, and $\omega_i = 2 \cdot \pi \cdot 50$: (a) the circular trajectory, Wachspress barycentric coordinates method, (b) the circular trajectory, virtual–zero component method, (c) the straight–line trajectory, Wachspress barycentric coordinates method, (d) NTV–PWM approach.

TABLE 4. Calculated Total Harmonic Distortion (THD) of v_{o1} for modulation methods shown in Fig. 40, $T_S = 200\mu s$, $\phi_i = 0$.

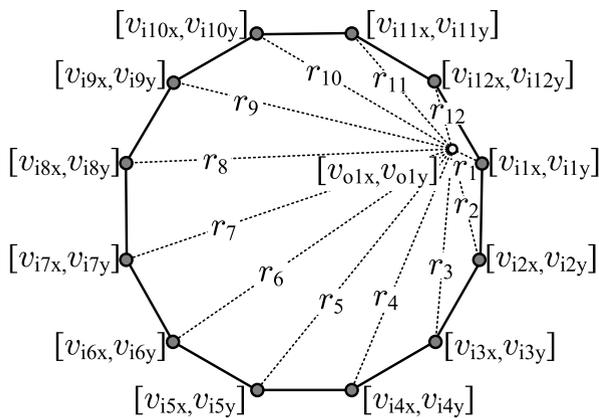| THD	(a)	(b)	(c)	(d)
$\omega_o = \omega_i$	41%	44%	55%	36%
$\omega_o = 5 \cdot \omega_i$	35%	37%	51%	31%

FIGURE 41. Synthesis field of the 12 × 12 matrix topology.

The presented method of computing the PWM duty cycles for a five–phase input converter can be successfully extended to the other matrix converters with a greater number of inputs. A new concept of power flow control in a power system transmission line by a new Flexible AC Transmission Systems (FACTS) device, which contains two power transformers and a multiphase matrix converter as an active control unit was proposed in papers [55], [56]. However, the authors
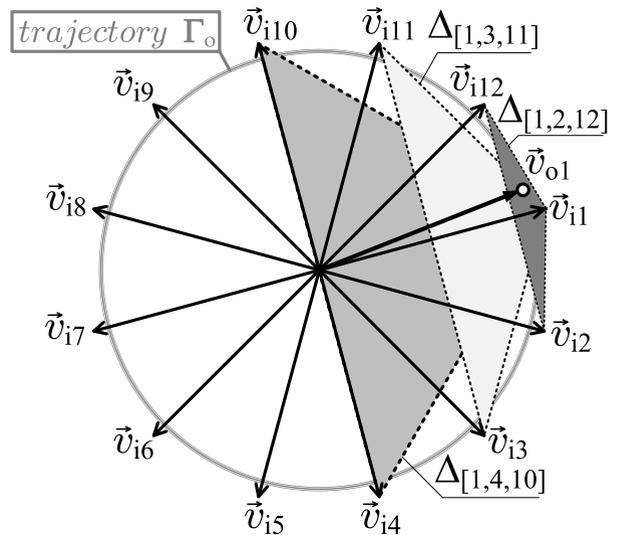

FIGURE 42. Input voltage vectors and an example reference output voltage $\vec{v}_{o1}$ with its circle trajectory Γ_o.

TABLE 5. Three considered methods of the input angle ϕ_i control.

control by the γ ratio factor (see Fig. 43)	
	$\mathbf{D} = \gamma \mathbf{D}_+ + (1 - \gamma)\mathbf{D}_-$ $\gamma \in \langle 0, 1 \rangle$ $\mathbf{D}_+ = f(\bar{\mathbf{v}}_{o+})$ $\mathbf{D}_- = f(\bar{\mathbf{v}}_{o-})$ $\phi_i \in \langle -\varphi_L, +\varphi_L \rangle$ $\phi_i = f(\gamma)$
the input angle control using the sequence type toggling (see Fig. 45)	
	$\mathbf{D} = \mathbf{D}_+$ $\Leftrightarrow 0 < t < \delta T_{\mathrm{PWM}}$ $\mathbf{D} = \mathbf{D}_-$ $\Leftrightarrow \delta T_{\mathrm{PWM}} \leq t < T_{\mathrm{PWM}}$ $\delta \in \langle 0, 1 \rangle$ $\mathbf{D}_+ = f(\bar{\mathbf{v}}_{o+})$ $\mathbf{D}_- = f(\bar{\mathbf{v}}_{o-})$ $\phi_i \in \langle -\varphi_L, +\varphi_L \rangle$ $\phi_i = f(\delta)$ $\phi_i = 0 \Leftrightarrow \delta = 0.5$
control by the rotation matrix $\mathbf{R}$ (see Fig. 44)	
	$\bar{\mathbf{v}}_{i\phi} = \bar{\mathbf{v}}_i \mathbf{R}$ $\mathbf{R} = \begin{bmatrix} \cos(\phi_i), -\sin(\phi_i) \\ \sin(\phi_i), \cos(\phi_i) \end{bmatrix}$ $\mathbf{D}_+ = f(\bar{\mathbf{v}}_{o+}, \bar{\mathbf{v}}_{i\phi})$ $\mathbf{D}_- = f(\bar{\mathbf{v}}_{o-}, \bar{\mathbf{v}}_{i\phi})$ $\mathbf{D} = 0.5(\mathbf{D}_+ + \mathbf{D}_-)$ $\phi_i \in \langle -0.5\pi, +0.5\pi \rangle$ $q_{\max} = \cos\left(\frac{\pi}{k}\right) \cdot \cos(\phi_i)$

did not propose a technique of the voltage modulation than the control for the cycloconverter. Therefore, the further text presents a PWM modulation based on the NTV approach applied to the CMC12 × 12. Now let's consider the graphical vector arrangements for 12×12 topology expressed as regular polygon shown in Fig. 41. One of 12 presented input vectors is referred here as the *base vector*. It means that the distance – defined as $r_1 \cdots r_{12}$ and shown in Fig. 42 – between this vector and the reference vector $\vec{v}_{o1}$ is the smallest.
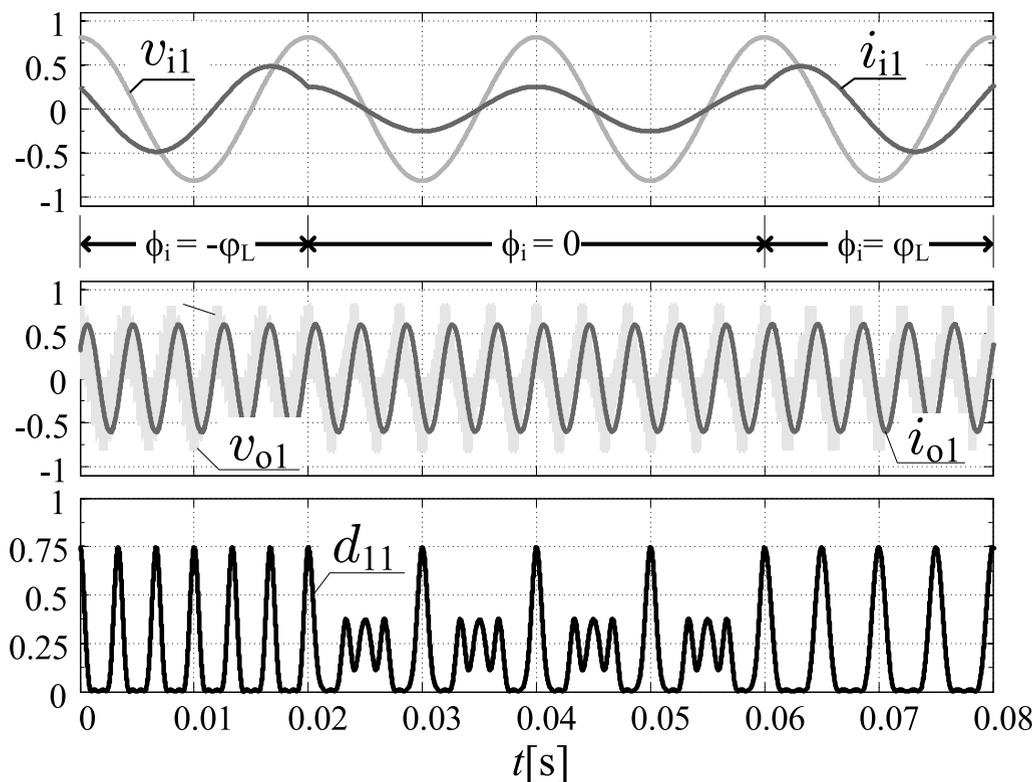
FIGURE 43. An input angle control by adjusting the γ ratio factor for CMC5 × 5: $q = 0.8$, $\omega_o = 5 \cdot \omega_i$, and $\omega_i = 2 \cdot \pi \cdot 50$.

There are three triangles with a common upper vertex with coordinates $\{v_{i1x}, v_{i1y}\}$: $\Delta_{[2,1,12]}$, $\Delta_{[3,1,11]}$, and $\Delta_{[4,1,10]}$. The given triangle $\Delta_{[p,q,r]}$ satisfies the modulation conditions when the sum

$$\Sigma_{[p,q,r]} = d_p + d_q + d_r \tag{51}$$

where

$$\begin{bmatrix} d_p \\ d_q \\ d_r \end{bmatrix} = \xi \begin{bmatrix} \left| \det \begin{bmatrix} v_{qx} - v_{o1x} & v_{qy} - v_{o1y} \\ v_{rx} - v_{o1x} & v_{ry} - v_{o1y} \end{bmatrix} \right| \\ \left| \det \begin{bmatrix} v_{px} - v_{o1x} & v_{py} - v_{o1y} \\ v_{rx} - v_{o1x} & v_{ry} - v_{o1y} \end{bmatrix} \right| \\ \left| \det \begin{bmatrix} v_{qx} - v_{o1x} & v_{qy} - v_{o1y} \\ v_{px} - v_{o1x} & v_{py} - v_{o1y} \end{bmatrix} \right| \end{bmatrix} \tag{52}$$

and

$$\xi = \left| \det \begin{bmatrix} v_{px} - v_{qx} & v_{py} - v_{qy} \\ v_{rx} - v_{qx} & v_{ry} - v_{qy} \end{bmatrix} \right|^{-1} \tag{53}$$

of PWM duty cycles d_p, d_q, and d_r takes the smallest value, ideally equal unity. When two triangles meet this condition, the one whose area, the triangle with the smallest area should be selected for further consideration. In practice, this operation can be performed by using optimized DSP functions like *qsort*, *vecmin* or conditional operators. The gate signals control can be performed by the MMM method, which is similar to Cyclic Venturini method described in [40]. When the value of transfer voltage ratio q is in the range

$$\frac{\cos\left(\frac{\pi}{6}\right)}{\cos\left(\frac{\pi}{12}\right)} \leq q \leq \cos\left(\frac{\pi}{12}\right) \tag{54}$$

large number of output phases allows generating the output voltage with lower THD, thus the cost of passive elements can be also reduced.

B. AN INPUT ANGLE CONTROL SCHEMES FOR MULTIPHASE CMCM × M FOR THE CIRCULAR TRAJECTORY OF THE MODULATING SIGNAL

The control of the input angle ϕ_i, defined as the displacement between the input voltage and the input current, is an important feature of the matrix converter control algorithm [1]–[3], [32]. Therefore some existing classic approaches have been considered and adopted for the multiphase CMC$m \times m$. Table 5 illustrates and gives the fundamental formulas for three methods of control input angle ϕ_i.

Figures shown in Table 5 demonstrate the input angle control methods for CMC12 × 12. These methods can be applied to another number of phases as well. The first characterized method of ϕ_i control is realized by setting the γ ratio factor. The PWM duty cycle m–degree matrix $\mathbf{D}_+$ is calculated for the circular trajectory of the modulating signal and output vectors rotating clockwise. The $\mathbf{D}_-$ indicates the same collection but calculated for counterclockwise rotation. The input angle ϕ_i is theoretically equal to zero for the γ equal to 0.5. A selected currents and voltages waveforms for such kind of input angle control have been shown in Fig. 43, where the PWM duty cycle d_{11} has been also illustrated. All required PWM duty cycles have been calculated using the Wachspress barycentric coordinates. The simulation has been performed
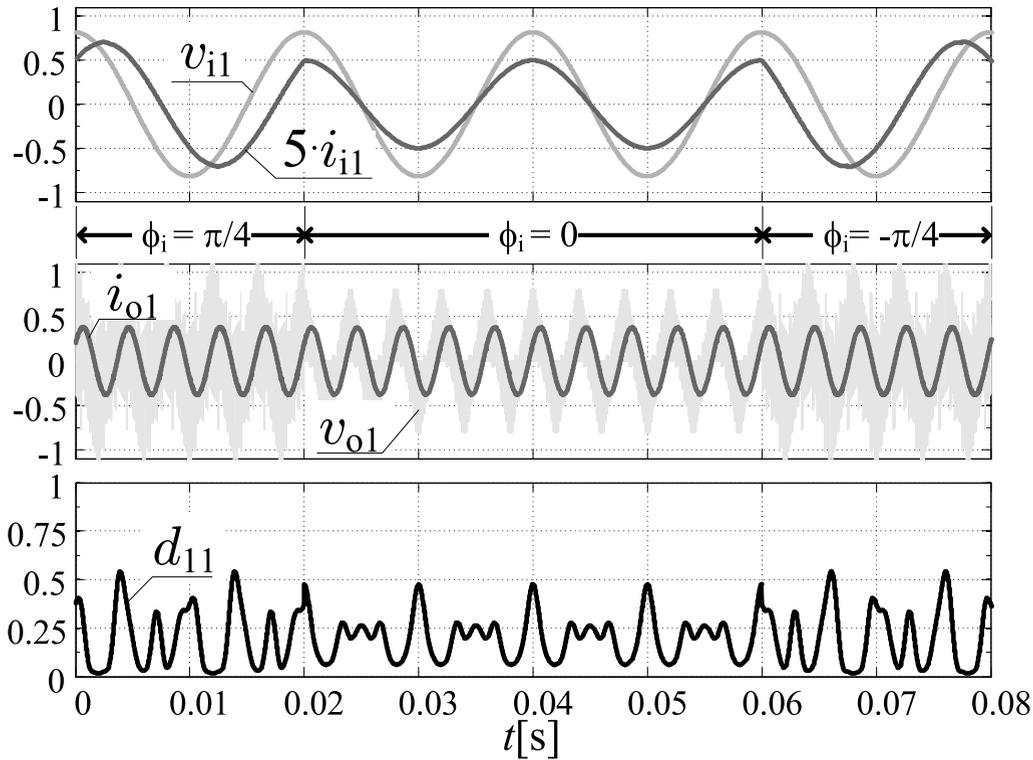
FIGURE 44. An input angle control using the rotation matrix R for CMC5 × 5: $q = 0.4$, $\omega_o = 5 \cdot \omega_i$, and $\omega_i = 2 \cdot \pi \cdot 50$.
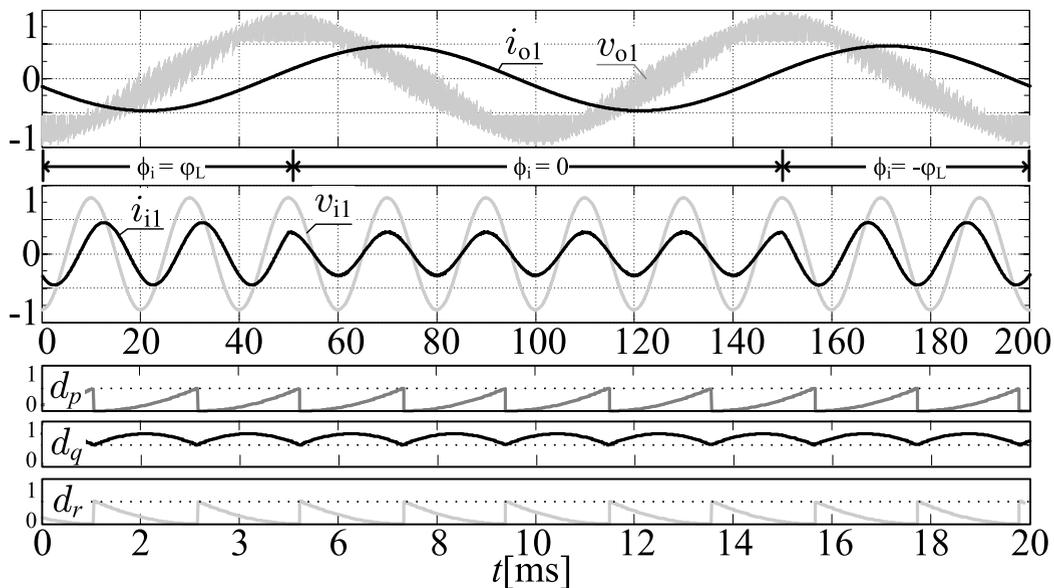
FIGURE 45. The input angle control using the sequence type toggling for CMC12 × 12 converter connected with RL load: $q = 0.95$, $\omega_i = 5\omega_o$.

for RL type of load and all electrical waveforms have been presented in p.u. units.

If the extended range of input angle control is needed the scheme with rotation matrix **R** usage can be applied. The proposed control of the input angle has been based on the rotated collection of input voltage vectors by a rotation matrix. In consequence, the real maximum voltage transfer ratio q has been reduced depending on the cosine of the

desired input angle ϕ_i, as presented in Table 5. Example simulation results are presented in Fig. 44.

The NTV requires a proper selection of three input vectors. There are two collections of rotating input vectors in the proposed method. Both collections can be used for the synthesis of the output voltage within the modulation period. The input angle can be adjusted by setting a ratio factor δ, as has been also presented in the Table 5. Simulation results

FIGURE 46. Direct voltage synthesis using the circular trajectory of the modulating signal performed by CMC5 × 3 converter: $q = 0.8$, $\omega_o = \omega_i/3$, and $\omega_i = 2 \cdot \pi \cdot 50$.

FIGURE 47. Direct voltage synthesis using the circular trajectory of the modulating signal performed by CMC5 × 3 converter: $q = 0.8$, $\omega_o = 3 \cdot \omega_i$, and $\omega_i = 2 \cdot \pi \cdot 50$.
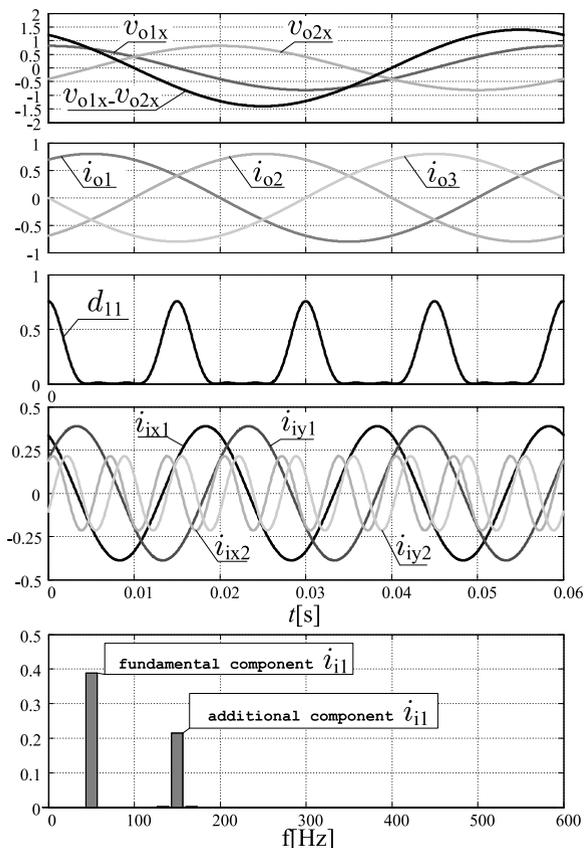
for the input angle control using the sequence type toggling for CMC12 × 12 converter are shown in Fig. 45. It has been found that for the circular trajectory of the modulating signal and an equal number of inputs and outputs, sinusoidal input currents can be obtained.

The first two methods of control the input angle maintain the maximum voltage transfer ratio q, but the adjustment range strongly depends on the load parameters. This type of control is needed when the purpose of the converter is to generate reactive power. The use of a rotation matrix R permits for the wider adjustment of the input angle ϕ_i. However, using this technique can decrease the q_{max} value.

The simulation result for $\omega_o = \omega_i/3$ is presented in Fig. 46, and the next case for $\omega_o = 3 \cdot \omega_i$ is illustrated in Fig. 47. Worth noting is that both input current components have been sinusoidal for the circular trajectories and the maximum transfer voltage ratio cannot exceed 0.809 value.

C. THE CHARACTERISTIC OF THE DIRECT MODULATION FOR CMC5 × 3

Compare to the classical 3×3 and $m \times m$ topologies, the disequality between the input and output voltage numbers create other conditions for the direct AC–AC voltage conversion. Some important properties of application two types of

modulating signals, the circular and the straight–line, have been analyzed in the subsection. Let's start an analysis from shortly defines two fundamental equations – for converter voltages

$$\begin{bmatrix} v_{o1x} \\ v_{o2x} \\ v_{o3x} \end{bmatrix}^T = \begin{bmatrix} v_{i1x} \\ v_{i2x} \\ v_{i3x} \\ v_{i4x} \\ v_{i5x} \end{bmatrix}^T \cdot \begin{bmatrix} d_{11} & d_{12} & d_{13} \\ d_{21} & d_{22} & d_{23} \\ d_{31} & d_{32} & d_{33} \\ d_{41} & d_{42} & d_{43} \\ d_{51} & d_{52} & d_{53} \end{bmatrix} \quad (55)$$

and for converter currents

$$\begin{bmatrix} i_{i1} \\ i_{i2} \\ i_{i3} \\ i_{i4} \\ i_{i5} \end{bmatrix}^T = \begin{bmatrix} i_{o1} \\ i_{o2} \\ i_{o3} \end{bmatrix}^T \cdot \begin{bmatrix} d_{11} & d_{21} & d_{31} & d_{41} & d_{51} \\ d_{12} & d_{22} & d_{32} & d_{42} & d_{52} \\ d_{13} & d_{23} & d_{33} & d_{43} & d_{53} \end{bmatrix}$$

$$(56)$$

The PWM duty cycle collection $d_{11} - d_{53}$ can be calculated using the Wachspress full form (23) or simplified (45) due to the input voltage symmetry assumption. This computation method has been applied to both types of trajectory,

FIGURE 48. Direct voltage synthesis using the straight–line trajectory of the modulating signal performed by CMC5 × 3 converter: $q = 0.8$, $\omega_o = 5 \cdot \omega_i$, and $\omega_i = 2 \cdot \pi \cdot 50$.
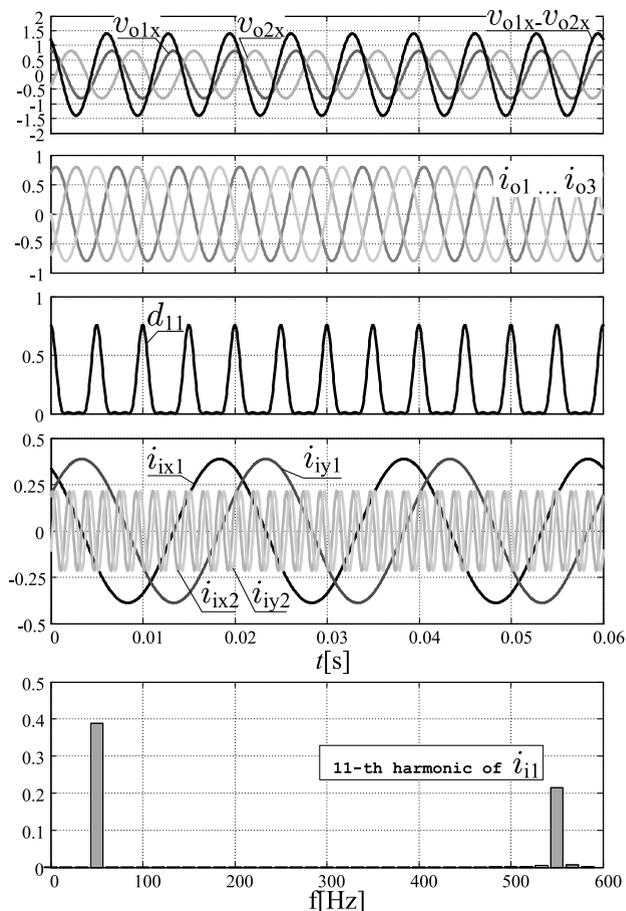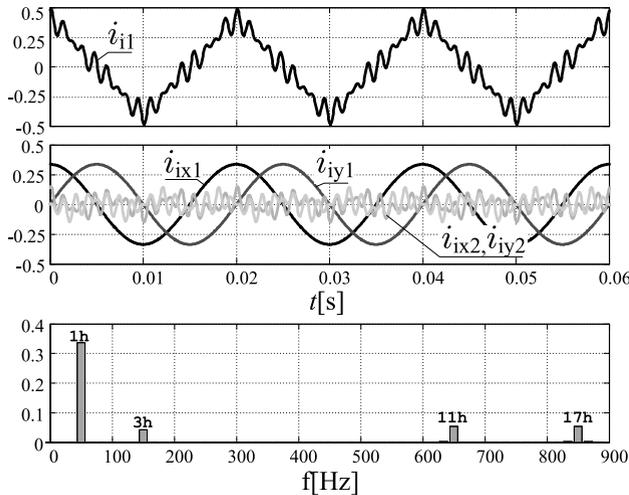

FIGURE 49. Optimized direct voltage synthesis using the straight–line trajectory of the modulating signal performed by CMC5 × 3 converter: $q = 1.04$, $\omega_o = \omega_i/3$, and $\omega_i = 2 \cdot \pi \cdot 50$.

thus the maximum voltage transfer ratios, represented by the equations (42) and (43) respectively, could be successfully obtained. However, the pure sinusoidal input currents have not been reached by the proposed solution. Therefore, for the further presentation of the input current, the following extended Clarke transformation for five–phase system has been used

$$\mathbf{C} = \frac{2}{5} \cdot \begin{bmatrix} 1 & \cos(\alpha) & \cos(2\alpha) & \cos(3\alpha) & \cos(4\alpha) \\ 0 & \sin(\alpha) & \sin(2\alpha) & \sin(3\alpha) & \sin(4\alpha) \\ 1 & \cos(2\alpha) & \cos(4\alpha) & \cos(6\alpha) & \cos(8\alpha) \\ 0 & \sin(2\alpha) & \sin(4\alpha) & \sin(6\alpha) & \sin(8\alpha) \\ \frac{1}{2} & \frac{1}{2} & \frac{1}{2} & \frac{1}{2} & \frac{1}{2} \end{bmatrix}$$
(57)

where $\alpha = 2 \cdot \pi/5$. Input currents can be presented in two ortogonal reference frames {x1, y1} and {x2, y2} using following expression

$$\begin{bmatrix} i_{ix1} \\ i_{iy1} \\ i_{ix2} \\ i_{iy2} \\ i_{i0} \end{bmatrix}^T = \begin{bmatrix} i_{i1} \\ i_{i2} \\ i_{i3} \\ i_{i4} \\ i_{i5} \end{bmatrix}^T \cdot \mathbf{C}$$
(58)

All presented results are prepared using MATLAB scripts and PSIM11 software. The MMM method of gate signal sequencing within a commutation group has been adopted. Only the pure sinusoidal reference output voltage was considered during research. In the case of the circular trajectory of the modulating signal application the input currents, averaged for the given modulation period, have contained fundamental and additional components. Two current harmonics were observed in all simulation results performed for the circular trajectory. If the input voltage vectors collection and the reference output voltage vectors collection are rotating in the opposite direction, the frequency of the input current
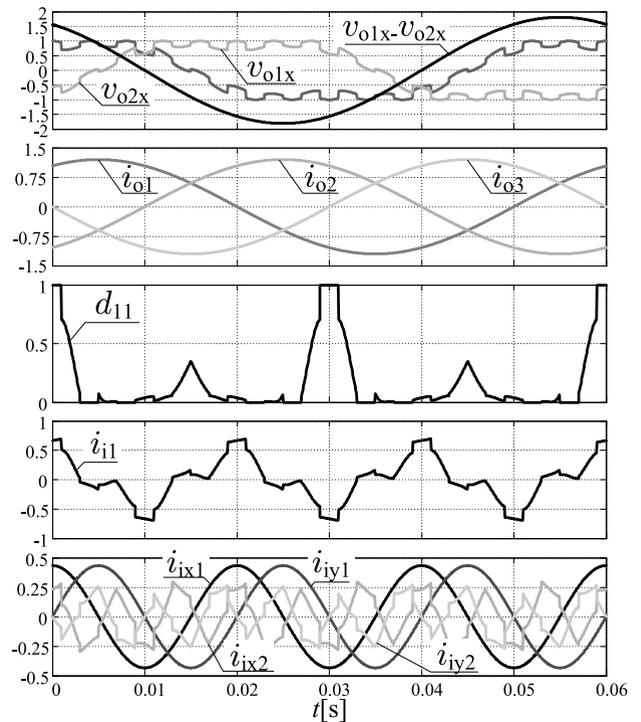
additional component can be expressed as follows

$$\omega_{\{x2,y2\}} = \omega_i \cdot \left(3 \cdot \frac{\omega_o}{\omega_i} + 2 \right)$$
(59)

If all vectors involved into AC–AC synthesis rotates in the same direction, the additional component pulsation can be written as

$$\omega_{\{x2,y2\}} = \omega_i \cdot \left(3 \cdot \frac{\omega_o}{\omega_i} - 2 \right)$$
(60)

The straight–line trajectory can be selected for obtaining a zero input angle but the accurate analytical characterization of the input current harmonic spectrum has not been made yet due to the overall complexity. The simulation result for $\omega_o = 5 \cdot \omega_i$ is presented in Fig. 48, where the input current can be also seen. This type of trajectory can be selected to increase the maximum voltage transfer ratio to the 1.044 value. The goal can be reached using the trajectory displacement to the optimal vertex of the synthesis field. This displacement guarantees that the real part value of the analytic signals is limited by the input voltages envelopes. The second important modification relies on the standard common–mode signal injection into output references. The simulation result for $\omega_o = \omega_i/3$ shown in Fig. 49.

VI. CONCLUSION
The paper introduces the alternative approach to the PWM duty cycle computation for the direct modulation in conventional matrix converters using analytical signals and

barycentric coordinates. The AC voltage sources are presented as a collection of the rotating vectors with coordinates obtained using the analytical signal concept. The several techniques of the analytic signal generation have also been discussed. The input vectors' arrangement has been replaced by the equivalent *synthesis field*, which is a convex polygon with vertices described by two–dimensional coordinates contain the *real*, and the *imaginary* component.

All reference output voltages are presented as points described also by a coordinates pair. These points reside inside the synthesis field by the introduced definition. The output voltage generated by the matrix converter is dependent on the real coordinates only. Thus the imaginary coordinates can be taken theoretically variable values. However, each modification of the analytic signal, which corresponds to the reference output vector, must not move any points outside the synthesis field. This modification can be presented by the *trajectory* – in particular as the straight and the circular line.

Finally, the synthesis field and the points, which represent the reference output voltages, form a graphical domain of the proposed solution. The PWM duty cycle modulation can be calculated using the barycentric coordinates theory. The mathematical relationship between the input and output quantities has been formulated using smooth interpolation methods. As the paper presents, these methods, have been reduced into a simple ratio of triangle areas. The goal has been reached by using the determinant of the two–dimensional matrix. Thus, trigonometry has been significantly limited in the algorithm.

The advantages of the proposed method, such as unification and universality, appear in the case of asymmetrical supply voltages or voltages with a shape different from sinusoidal. Until the Hibert transform or the quadrature component of the input voltages is calculated accurately, any input voltage can be used for the output voltage synthesis. The proposed method can be not only applied to a wide range of waveforms. As demonstrated, the synthesis field can be chosen arbitrally. The paper also discusses this context. The proposed approach can be applied for abnormal or non–standard voltage sources without the major changes in the algorithm.

The direct modulation for CMC3 $\times$ *n* has been also presented in the paper and proposed solution can be used in multiphase electric drive application. Again, the expained approach to modulation can be applied to the abnormal or non–standard AC voltage sources.

The concept of multiphase voltage synthesis based on the CMC*m* $\times$ *m* was introduced and verified by the analytical and simulation research. Three voltage synthesis schemes and a couple selected input angle control method were develop and proposed for multiphase systems.

The last fragment of consideration was dedicated to the problem of direct PWM modulation for CMC5 $\times$ 3. The desired output voltage is properly generated using the proposed approach but the (filtered, averaged) input current shape is not purely sinusoidal. The investigation of the apropriate modification of the modulating signal is currently ongoing.

The main purpose of the article was reducing the multiphase voltage synthesis algorithm complexity and formulate the direct synthesis rules. All proposals have been verified and successfully confirmed. Authors believe that due to trigonometry amount reduction and a new look on the modulation, the algorithms prototyping will be improved.

The presented paper does not include the high–order harmonic analysis because it strongly depends on the chosen switching sequence – Cyclic Venturini, MMM, etc. – and a number of parameters. However, the paper authors would like to present a selected variant of PWM modulation with high-order harmonic analysis in the other paper.

As mentioned in the paper, the computation scheme can be realized using the FPGA device only. Such research will be taken in the near future. The comparison with the space–vector approach will be also performed.

APPENDIX 1. AN ANALYSIS SCRIPT FOR USING WITH THE MATLAB SYMBOLIC MATH TOOLBOX

This script allows to modify both the input and the output voltages given in the analytic form. The PWM duty cycles d_{11}–d_{33} are calculated using the barycentric coordinates. For three inputs case, these operations are performed using the triangle area. The following script shows the theoretical expression of PWM duty cycles, which finally leads to the proof of the sinusoidal output voltage.

```
1   %init
2   clc;
3   close all;
4   clear all;
5   %symbolic time
6   t=sym('t','positive');
7   %symbolic data for input voltages
8   omega_i=sym('omega_i','positive');
9   %analytic form of input voltages
10  vi1_=exp(1i*omega_i*t);
11  vi2_=exp(1i*(omega_i*t-2*pi/3));
12  vi3_=exp(1i*(omega_i*t+2*pi/3));
13  %symbolic data for output voltages
14  q=sym('q');
15  assume(q < 0.5 & q > 0.0);
16  omega_o=sym('omega_o','positive');
17  %analytic form of input voltages
18  vo1_=q*exp(1i*omega_o*t);
19  vo2_=q*exp(1i*(omega_o*t-2*pi/3));
20  vo3_=q*exp(1i*(omega_o*t+2*pi/3));
21  %input coordinates
22  vi1x=real(vi1_);vi1y=imag(vi1_);
23  vi2x=real(vi2_);vi2y=imag(vi2_);
24  vi3x=real(vi3_);vi3y=imag(vi3_);
25  %output coordinates
26  vo1x=real(vo1_);vo1y=imag(vo1_);
27  vo2x=real(vo2_);vo2y=imag(vo2_);
28  vo3x=real(vo3_);vo3y=imag(vo3_);
29  %normalization factor
30  eta=det([vi1x vi1y 1;
31       vi2x vi2y 1;
32       vi3x vi3y 1]);
33  %PWM duty cycles computing
34  d11=det([vo1x vo1y 1;
35       vi2x vi2y 1;
36       vi3x vi3y 1])/eta;
37  d12=det([vo2x vo2y 1;
38       vi2x vi2y 1;
39       vi3x vi3y 1])/eta;
40  d13=det([vo3x vo3y 1;
41       vi2x vi2y 1;
42       vi3x vi3y 1])/eta;
43  d21=det([vi1x vi1y 1;
44       vo1x vo1y 1;
45       vi3x vi3y 1])/eta;
46  d22=det([vi1x vi1y 1;
47       vo2x vo2y 1;
48       vi3x vi3y 1])/eta;
49  d23=det([vi1x vi1y 1;
50       vo3x vo3y 1;
51       vi3x vi3y 1])/eta;
52  d31=det([vi1x vi1y 1;
53       vi2x vi2y 1;
```

```
54            volx voly 1])/eta;
55 d32=det([vi1x vi1y 1;
56            vi2x vi2y 1;
57            vo2x vo2y 1])/eta;
58 d33=det([vi1x vi1y 1;
59            vi2x vi2y 1;
60            vo3x vo3y 1])/eta;
61 %display results
62 pretty(simplify(d11));
63 pretty(simplify(d21));
64 pretty(simplify(d31));
65 pretty(simplify(d11+d21+d31));
66 pretty(simplify(d12+d22+d32));
67 pretty(simplify(d13+d23+d33));
68 %calculation of the real output voltages
69 vo1=d11*vi1x+d21*vi2x+d31*vi3x;
70 vo2=d12*vi1x+d22*vi2x+d32*vi3x;
71 vo3=d13*vi1x+d23*vi2x+d33*vi3x;
72 %display results
73 pretty(simplify(vo1));
74 pretty(simplify(vo2));
75 pretty(simplify(vo3));
76 %theoretical output currents
77 angle_o=sym('angle_o','positive');
78 Imax=sym('Imax','positive');
79 io1=Imax*cos(omega_o*t-angle_o);
80 io2=Imax*cos(omega_o*t-angle_o-2*pi/3);
81 io3=Imax*cos(omega_o*t-angle_o+2*pi/3);
82 %calculation of the real input currents
83 ii1=d11*io1+d12*io2+d13*io3;
84 ii2=d21*io1+d22*io2+d23*io3;
85 ii3=d31*io1+d32*io2+d33*io3;
86 %display results
87 pretty(simplify(ii1));
88 pretty(simplify(ii2));
89 pretty(simplify(ii3));
```

REFERENCES

[1] J. Rodriguez, M. Rivera, J. W. Kolar, and P. W. Wheeler, "A review of control and modulation methods for matrix converters," *IEEE Trans. Ind. Electron.*, vol. 59, no. 1, pp. 58–70, Jan. 2012.

[2] L. Helle, K. Larsen, A. Jorgensen, S. Munk-Nielsen, and F. Blaabjerg, "Evaluation of modulation schemes for three-phase to three-phase matrix converters," *IEEE Trans. Ind. Electron.*, vol. 51, no. 1, pp. 158–171, Feb. 2004.

[3] T. Friedli and J. Kolar, "Milestones in matrix converter research," *IEEJ J. Ind. Appl.*, vol. 1, no. 1, pp. 2–14, Jul. 2012.

[4] S. Mori, M. Aketa, T. Sakaguchi, H. Asahara, T. Nakamura, and T. Kimoto, "Suppression of punch-through current in 3 kV 4H-SiC reverse-blocking MOSFET by using highly doped drift layer," *IEEE J. Electron Devices Soc.*, vol. 6, no. 1, pp. 449–453, Mar. 2018.

[5] J. Luo, X.-P. Zhang, and Y. Xue, "Small signal model of modular multilevel matrix converter for fractional frequency transmission system," *IEEE Access*, vol. 7, pp. 110187–110196, 2019.

[6] S. Tammaruckwattana, C. Yue, Y. Ikeda, and K. Ohyama, "Comparison of switching losses of matrix converters for commutation methods," in *Proc. 16th Eur. Conf. Power Electron. Appl.*, Aug. 2014, pp. 1–10.

[7] Y. Guo, Y. Guo, W. Deng, J. Zhu, and F. Blaabjerg, "An improved 4-step commutation method application for matrix converter," in *Proc. 17th Int. Conf. Electr. Mach. Syst. (ICEMS)*, Oct. 2014, pp. 3590–3593.

[8] O. Simon, J. Mahlein, M. Muenzer, and M. Bruckmarm, "Modern solutions for industrial matrix-converter applications," *IEEE Trans. Ind. Electron.*, vol. 49, no. 2, pp. 401–406, Apr. 2002.

[9] A. Hassan, Y. Savaria, and M. Sawan, "GaN integration technology, an ideal candidate for high-temperature applications: A review," *IEEE Access*, vol. 6, pp. 78790–78802, 2018.

[10] M. Ishida, T. Ueda, T. Tanaka, and D. Ueda, "GaN on Si technologies for power switching devices," *IEEE Trans. Electron Devices*, vol. 60, no. 10, pp. 3053–3059, Oct. 2013.

[11] D. Lan, P. Das, and S. K. Sahoo, "A high-frequency link matrix rectifier with a pure capacitive output filter in a discontinuous conduction mode," *IEEE Trans. Ind. Electron.*, vol. 67, no. 1, pp. 4–15, Jan. 2020.

[12] R. J. Kaplar, M. J. Marinella, S. DasGupta, M. A. Smith, S. Atcitty, M. Sun, and T. Palacios, "Characterization and reliability of SiC- and gan-based power transistors for renewable energy applications," in *Proc. IEEE Energytech*, May 2012, pp. 1–6.

[13] J. Benzaquen, M. B. Shadmand, and B. Mirafzal, "Ultrafast rectifier for variable-frequency applications," *IEEE Access*, vol. 7, pp. 9903–9911, 2019.

[14] Q. Wu, M. Wang, W. Zhou, X. Wang, G. Liu, and C. You, "Analytical switching model of a 1200 V SiC MOSFET in a high-frequency series resonant pulsed power converter for plasma generation," *IEEE Access*, vol. 7, pp. 99622–99632, 2019.

[15] P. W. Wheeler, J. C. Clare, M. Apap, D. Lampard, S. J. Pickering, K. J. Bradley, and L. Empringham, "An integrated 30 kw matrix converter based induction motor drive," in *Proc. IEEE 36th Power Electron. Spec. Conf.*, Jun. 2005, pp. 2390–2395.

[16] L. Empringham, J. W. Kolar, J. Rodriguez, P. W. Wheeler, and J. C. Clare, "Technological issues and industrial application of matrix converters: A review," *IEEE Trans. Ind. Electron.*, vol. 60, no. 10, pp. 4260–4271, Oct. 2013.

[17] L. R. Merchan-Villalba, J. M. Lozano-Garcia, J. G. Avina-Cervantes, H. J. Estrada-Garcia, and J. Martinez-Patino, "Matrix converter based on SVD modulation using a microcontroller as unique controlling device," *IEEE Access*, vol. 7, pp. 164815–164824, 2019.

[18] K. Rahman, A. Iqbal, M. A. Al-Hitmi, O. Dordevic, and S. Ahmad, "Performance analysis of a three-to-five phase dual matrix converter based on space vector pulse width modulation," *IEEE Access*, vol. 7, pp. 12307–12318, 2019.

[19] S. M. Ahmed, A. Iqbal, and H. Abu-Rub, "Generalized duty-ratio-based pulsewidth modulation technique for a three-to-k phase matrix converter," *IEEE Trans. Ind. Electron.*, vol. 58, no. 9, pp. 3925–3937, Sep. 2011.

[20] A. Iqbal, H. Abu-Rub, J. Rodriguez, C. A. Rojas, and M. Saleh, "Simple carrier-based PWM technique for a three-to-nine-phase direct AC–AC converter," *IEEE Trans. Ind. Electron.*, vol. 58, no. 11, pp. 5014–5023, Nov. 2011.

[21] S. M. Ahmed, Z. Salam, and H. Abu-Rub, "An improved space vector modulation for a three-to-seven-phase matrix converter with reduced number of switching vectors," *IEEE Trans. Ind. Electron.*, vol. 62, no. 6, pp. 3327–3337, Jun. 2015.

[22] X. Wang, H. Lin, H. She, and B. Feng, "A research on space vector modulation strategy for matrix converter under abnormal input-voltage conditions," *IEEE Trans. Ind. Electron.*, vol. 59, no. 1, pp. 93–104, Jan. 2012.

[23] W. Xiong, Y. Sun, J. Lin, M. Su, H. Dan, M. Rivera, and J. M. Guerrero, "A cost-effective and low-complexity predictive control for matrix converters under unbalanced grid voltage conditions," *IEEE Access*, vol. 7, pp. 43895–43905, 2019.

[24] Z. Malekjamshidi, M. Jafari, and J. Zhu, "Analysis and comparison of direct matrix converters controlled by space vector and Venturini modulations," in *Proc. IEEE 11th Int. Conf. Power Electron. Drive Syst.*, Jun. 2015, pp. 635–639.

[25] A. K. Dey, G. Mohapatra, T. K. Mohapatra, and R. Sharma, "A modified Venturini PWM scheme for matrix converters," in *Proc. IEEE Int. Conf. Sustain. Energy Technol. Syst. (ICSETS)*, Feb. 2019, pp. 013–018.

[26] Z. Malekjamshidi, M. Jafari, J. Zhu, and D. Xiao, "Comparative analysis of input power factor control techniques in matrix converters based on model predictive and space vector control schemes," *IEEE Access*, vol. 7, pp. 139150–139160, 2019.

[27] S. Feng, J. Lei, J. Zhao, W. Chen, and F. Deng, "Improved reference generation of active and reactive power for matrix converter with model predictive control under input disturbances," *IEEE Access*, vol. 7, pp. 97001–97012, 2019.

[28] E. Levi, "Multi-phase machines for variable speed applications," *IEEE Trans. Ind. Electron.*, vol. 55, no. 5, pp. 1893–1909, May 2008.

[29] E. Levi, R. Bojoi, F. Profumo, H. Toliyat, and S. Williamson, "Multi-phase induction motor drives-a technology status review," *IET Electr. Power Appl.*, vol. 1, no. 4, pp. 489–516, Jul. 2007.

[30] O. Abdel-Rahim, H. Funato, H. Abu-Rub, and O. Ellabban, "Multiphase wind energy generation with direct matrix converter," in *Proc. IEEE Int. Conf. Ind. Technol. (ICIT)*, Feb. 2014, pp. 519–523.

[31] D. Casadei, G. Serra, A. Tani, and L. Zarri, "Matrix converter modulation strategies: A new general approach based on space-vector representation of the switch state," *IEEE Trans. Ind. Electron.*, vol. 49, no. 2, pp. 370–381, Apr. 2002.

[32] H. Hojabri, H. Mokhtari, and L. Chang, "A generalized technique of modeling, analysis, and control of a matrix converter using SVD," *IEEE Trans. Ind. Electron.*, vol. 58, no. 3, pp. 949–959, Mar. 2011.

[33] M. Ali, A. Iqbal, M. R. Khan, M. Ayyub, and M. A. Anees, "Generalized theory and analysis of scalar modulation techniques for a $m \times n$ matrix converter," *IEEE Trans. Power Electron.*, vol. 32, no. 6, pp. 4864–4877, Jun. 2017.

[34] A. Reilly, G. Frazer, and B. Boashash, "Analytic signal generation-tips and traps," *IEEE Trans. Signal Process.*, vol. 42, no. 11, pp. 3241–3245, Nov. 1994.

[35] L. Marple, "Computing the discrete-time 'analytic' signal via FFT," *IEEE Trans. Signal Process.*, vol. 47, no. 9, pp. 2600–2603, Sep. 1999.

[36] L. Asiminoael, F. Blaabjerg, and S. Hansen, "Computing the discrete-time 'analytic' signal via FFT," *IEEE Ind. Appl. Mag.*, vol. 13, no. 4, pp. 22–33, Jul. 2007.

[37] P. Szczepankowski, P. Wheeler, and T. Bajdecki, "Application of analytic signal and smooth interpolation in pulse width modulation for conventional matrix converters," *IEEE Trans. Ind. Electron.*, to be published.

[38] P. Szczepankowski and J. Nieznanski, "Application of Barycentric coordinates in space vector PWM computations," *IEEE Access*, vol. 7, pp. 91499–91508, 2019.

[39] N. S. E. Malsch, "Recent advanced in the construction of polygonal finite element interpolants," *Arch. Comput. Methods Eng.*, vol. 11, pp. 1–38, Sep. 2005.

[40] M. Apap, J. Clare, P. Wheeler, and K. Bradley, "Analysis and comparison of AC–AC matrix converter control strategies," in *Proc. IEEE 34th Annu. Conf. Power Electron. Spec.*, Jun. 2003, pp. 1287–1292.

[41] G. Dasgupta, "Interpolants within convex polygons: Wachspress shape functions," *J. Aerosp. Eng.*, vol. 16, no. 1, pp. 1–8, Jan. 2003.

[42] G. Todoran and R. Holonec, "Analysis of the multi-phased system based on the concept of analytic signals," in *Proc. 4th Int. Conf. Power Eng., Energy Elect. Drives*, May 2013, pp. 664–669.

[43] C. Rader, "A simple method for sampling in-phase and quadrature components," *IEEE Trans. Aerosp. Electron. Syst.*, vol. AES-20, no. 6, pp. 821–824, Nov. 1984.

[44] X. Chen, J. Wang, V. I. Patel, and P. Lazari, "A nine-phase 18-slot 14-pole interior permanent magnet machine with low space harmonics for electric vehicle applications," *IEEE Trans. Energy Convers.*, vol. 31, no. 3, pp. 860–871, Sep. 2016.

[45] T. D. Nguyen and H.-H. Lee, "Development of a three-to-five-phase indirect matrix converter with carrier-based PWM based on space-vector modulation analysis," *IEEE Trans. Ind. Electron.*, vol. 63, no. 1, pp. 13–24, Jan. 2016.

[46] C. N. El-Khoury, H. Y. Kanaan, I. Mougharbel, and K. Al-Haddad, "A review of matrix converters applied to PMSG based wind energy conversion systems," in *Proc. 39th Annu. Conf. IEEE Ind. Electron. Soc. (IECON)*, Nov. 2013, pp. 7784–7789.

[47] X. Liu, P. Wang, P. C. Loh, and F. Blaabjerg, "A three-phase dual-input matrix converter for grid integration of two AC type energy resources," *IEEE Trans. Ind. Electron.*, vol. 60, no. 1, pp. 20–30, Jan. 2013.

[48] R. Pena, R. Cardenas, E. Reyes, J. Clare, and P. Wheeler, "Control of a doubly fed induction generator via an indirect matrix converter with changing DC voltage," *IEEE Trans. Ind. Electron.*, vol. 58, no. 10, pp. 4664–4674, Oct. 2011.

[49] A. Garcés and M. Molinas, "A study of efficiency in a reduced matrix converter for offshore wind farms," *IEEE Trans. Ind. Electron.*, vol. 59, no. 1, pp. 184–193, Jan. 2012.

[50] J. Esch, "High-power wind energy conversion systems: State-of-the-art and emerging technologies," *Proc. IEEE*, vol. 103, no. 5, pp. 736–739, May 2015.

[51] I. Zoric, M. Jones, and E. Levi, "Arbitrary power sharing among three-phase winding sets of multiphase machines," *IEEE Trans. Ind. Electron.*, vol. 65, no. 2, pp. 1128–1139, Feb. 2018.

[52] A. Iqbal, S. Moinuddin, M. R. Khan, S. M. Ahmed, and H. Abu-Rub, "A novel three-phase to five-phase transformation using a special transformer connection," *IEEE Trans. Power Del.*, vol. 25, no. 3, pp. 1637–1644, Jul. 2010.

[53] A. S. Abdel-Khalik, A. Elserougi, Z. Shafik, S. Ahmed, and A. Massoud, "A scott connection-based three-phase to five-phase power transformer," in *Proc. 39th Annu. Conf. IEEE Ind. Electron. Soc. (IECON)*, Nov. 2013, pp. 2559–2564.

[54] A. Munteanu, A. Simion, D. A. Hagianu, L. Livadaru, and D. Bidei, "Special three-phase to multiple different polyphase systems electric transformer," in *Proc. Int. Conf. Expo. Elect. Power Eng. (EPE)*, Oct. 2014, pp. 345–348.

[55] T. J. Sobczyk and D. Borkowski, "Application of matrix converter for power flow control in a transmission line," in *Proc. IEEE Lausanne Power Tech*, Jul. 2007, pp. 1823–1828.

[56] T. J. Sobczyk, T. Sienko, and J. B. Danilewicz, "Study of asymmetrical regimes in matrix converters for multi-phase high speed generators," in *Proc. IEEE Russia Power Tech*, Jun. 2005, pp. 1–6.

PAWEL SZCZEPANKOWSKI (Member, IEEE) received the Ph.D. degree in electrical engineering from the Gdansk University of Technology, Poland, in 2009. He has authored or coauthored more than 30 scientific and technical articles. His research interests include designs, control, diagnostics, modeling, and simulation of power electronic converters, including multilevel and matrix topologies, and signal processing with the use of advanced DSP and FPGA devices. He is a member of the Research and Development team of LINTE^2 Laboratory, Gdansk University of Technology.

TOMASZ BAJDECKI received the M.S. degree in electrical engineering from the Czestochowa University of Technology, Poland, in 1992, and the Ph.D. degree from the Gdansk University of Technology, in 2003. He is currently a Research Staff Member with the Institute of Power Engineering, Gdansk. His main current interest is in the area of control of the high-power converters. His Ph.D. Dissertation was on Control Strategy for the Matrix Converter.

RYSZARD STRZELECKI (Senior Member, IEEE) graduated in industrial electronics from the Kyiv University of Technology, in 1981. He received the Ph.D. degree, in 1984, and the Habilitation (D.Sc.) degree in the theme prediction control of the self-commutation power electronics converters from the Institute of Electrodynamics, Academy of Sciences, Ukrainian Soviet Socialist Republic, Kiev, in 1991. In 1999, he received the title of Professor of technical sciences. He is currently a Full Professor with the Gdansk University of Technology, Poland, and a Professor with the Lukasiewicz Research Network–Electrical Engineering Institute (Warsaw/Gdansk, Poland). He is the author of more scientific articles and monographs and patents. His interests focus on topologies and control methods and the industrial application of power electronic systems.

• • •